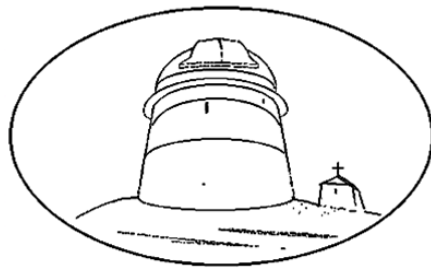


Physical processes effecting the baryonic matter content of the Universe



Mariana Panayotova Manusheva
Institute of Astronomy and National Astronomical Observatory
Bulgarian Academy of Sciences

PhD Thesis in Astrophysics and Stellar Astronomy, 01.04.02

2014

1. Scientific SUPERVISOR: Prof. Dr. Daniela Kirilova

2. Scientific Advisor: Prof. Dr. Georgi Petrov

Abstract

In this thesis we have discussed physical processes effecting the generation of the matter content of the Universe.

First, we have studied the processes effecting Big Bang Nucleosynthesis during which the chemical content of the baryonic component of the Universe was produced. We have provided detail numerical analysis of the BBN production of ${}^4\text{He}$, Y_p , in the presence of $\nu_e \leftrightarrow \nu_s$ neutrino oscillations, effective after electron neutrino decoupling. We have accounted for all known oscillations effects of neutrino oscillations on cosmological nucleosynthesis. We have calculated iso-helium contours and have obtained cosmological bounds corresponding to $\delta Y_p/Y_p = 5.2\%$ in correspondance with the recently found higher uncertainty in ${}^4\text{He}$. In the framework of our analysis, iso-helium contours for $\delta Y_p/Y_p > 5\%$ and different initial population of the sterile neutrino have been calculated, namely $\delta N_s = 0; 0.5; 0.7; 0.9$, both for resonant and non-resonant oscillations. The change of cosmological constraints in case of non-zero δN_s was determined. The results are important both for cosmology and for neutrino physics.

Further we have studied the processes effecting the formation of the baryon content of the Universe. We have constructed Scalar Field Condensate baryogenesis model based on Affleck and Dine baryogenesis scenario, which is consistent with the low energy required by inflation and can naturally produce the observed baryon asymmetry of the Universe. We have provided precise numerical analysis of the SFC baryogenesis model numerically accounting for the particle creation processes by the time varying scalar field. We have shown that there is a considerable difference in the obtained results compared to the analytical approach for the rate of particle creation Γ calculation. We have numerically obtained the dependence of the field and

baryon charge evolution and their final values on the model's parameters gauge coupling constant α , Hubble constant during inflation H_I , mass of the field m and self coupling constants λ_i . We have found the range of model parameters for which baryon asymmetry value close to the observed one can be generated. It has been shown that for a natural range of the model's parameters the inhomogeneous SCB model is able to predict astronomically interesting vast antimatter domains, separated from the matter ones by baryonically empty voids.

Acknowledgements

I am extremely grateful to Dr. Daniela Kirilova for her immense support as my supervisor. She has also been a friend to talk to and has always inspired and motivated me ever since my graduate years.

I would like to thank to Dr. Georgi Petrov, who was my supervisor during the first year and scientific advisor during the second year of my PhD. I would like to thank also to my colleagues from IA with NAO, who encouraged and supported me, and especially to Toni Valchanov and Valentin Kopchev. I am grateful to the IA for the opportunity to participate in conferences, where to present our results. I have to mention also Abdus Salam ISTEP, Trieste, Italy, where I was able to provide most of the numerical analysis, described in the second part of this PhD thesis.

Contents

List of Figures	v
List of Tables	viii
Introduction	1
Background and motivation	1
Aims and objectives	3
I Processes important for the formation of the chemical content of the Universe	5
1 Big Bang Nucleosynthesis theory and observations	6
1.1 Theoretical calculations of the primordial abundances of the light elements	10
1.2 Observational values of the primordial abundances of the light elements	11
1.2.1 Deuterium	11
1.2.2 Helium-3	11
1.2.3 Lithium-7	13
1.2.4 Helium-4	15
2 Neutrino and neutrino oscillations	19
2.1 Neutrino oscillations detection	19
2.1.1 Solar neutrino anomaly	19
2.1.2 Atmospheric neutrino anomaly	21
2.1.3 Accelerator neutrino experiments	21
2.2 Sterile neutrino	21
2.3 Neutrino oscillations parameters	23

2.4	Specifications of the BBN with electron-sterile neutrino oscillations model	23
2.5	Cosmological effects of neutrino oscillations	29
2.5.1	Dependence of Y_p on $\delta N_s \neq 0$ for the case, when $\delta Y_p/Y_p > 5\%$	30
3	BBN bounds on neutrino oscillations parameters	33
3.1	The case with empty initial population of the sterile neutrino, $\delta N_s = 0$	33
3.2	The case with non-zero initial population of the sterile neutrino, $\delta N_s \neq 0$	34
3.3	Discussion and conclusions	37
3.4	Future work	40
II	Processes important for the generation of the baryonic content of the Universe	42
4	Baryon asymmetry of the Universe	43
4.1	Cosmic and Gamma rays indications for matter domination in the Universe	43
4.2	Baryon density measurements	47
4.3	Baryogenesis models	48
5	Scalar field condensate baryogenesis scenario	51
5.1	Description and assumptions of the model	52
5.2	Numerical study of the scalar field and baryon number evolution	53
6	Results from the numerical analysis of the model	54
6.1	Role of particle creation processes	54
6.2	Dependence on the model parameters	55
6.2.1	Dependence on gauge coupling constant α	59
6.2.2	Dependence on Hubble constant during inflation H_I	59
6.2.3	Dependence on the mass m of the condensate	59
6.2.4	Dependence on self coupling constants λ_i	59
6.3	Inhomogenous scalar field condensate baryogenesis model	65
6.4	Discussion and conclusions	70
6.5	Future work	71
	Main results and contributions	75

CONTENTS

List of publications	77
Citations	80
Appendices	81
References	81

List of Figures

1.1	The evolution of primordial nuclei synthesis in SBBN model	9
1.2	D/H ratios for different QSO systems as a function of the redshift	12
1.3	${}^3\text{He}/\text{H}$ for observations with different metallicity	13
1.4	The Lithium abundance for different observational objects as a function of metallicity	14
1.5	The derivation of the primordial ${}^4\text{He}$ mass fraction	16
1.6	The abundances of light elements predicted by the SBBN model with 95% <i>C.L.</i> (wide bands) as a function of baryon to photon ratio η	17
2.1	Oscillation parameter δm^2 as a function of $\tan 2\theta$	24
2.2	The illustration of nonequilibrium neutrino oscillations effects on BBN.	28
2.3	The spectrum distortion at different degrees of population of the steriles	30
2.4	The dependence of the dynamical, kinetic and the total effect on δN_s value	31
3.1	BBN constraints for $\delta Y_p/Y_p = 5.2\%$ and different δN_s values	36
3.2	BBN constraints for $\delta Y_p/Y_p = 3\%$ and $\delta Y_p/Y_p = 5.2\%$	38
4.1	BESS 1995-2000 antiproton spectrum at the top of the atmosphere and CAPRICE and MASS data	45
6.1	Field and B evolution with analitically accounted particle creation processes. - The evolution of the scalar field $\varphi(\eta)$ and the baryon charge $B(\eta)$ for $\lambda_1 = 5 \times 10^{-2}$, $\lambda_2 = \lambda_3 = 5 \times 10^{-4}$, $\alpha = 10^{-3}$, $H = 10^{11}$ GeV, $m=350$ GeV, $\varphi_o = 2^{-1/4}H\lambda^{-1/4}$ and $\dot{\varphi}_o = H^2$ [1].	56

6.2	Field and B evolution with numerically accounted particle creation processes. - The evolution of the scalar field $\varphi(\eta)$ and baryon charge $B(\eta)$ for $\lambda_1 = 5 \times 10^{-2}$, $\lambda_2 = \lambda_3 = 5 \times 10^{-4}$, $\alpha = 10^{-3}$, $H = 10^{11}$ GeV, $m=350$ GeV, $\varphi_o = 2^{-1/4}H\lambda^{-1/4}$, and $\dot{\varphi}_o = H^2$ [1].	57
6.3	The evolution of the baryon charge $B(\eta)$ for $\lambda_1 = 5 \times 10^{-2}$, $\lambda_2 = \lambda_3 = 10^{-3}$, $\alpha = 10^{-2}$, $H = 10^{10}$ GeV, $m=350$ GeV, $\varphi_o = H_I\lambda^{-1/4}$ and $\dot{\varphi}_o = H_I^2$	58
6.4	The evolution of the baryon charge $B(\eta)$ for $\lambda_1 = 5 \times 10^{-2}$, $\lambda_2 = \lambda_3 = 10^{-3}$, $H = 10^{10}$ GeV, $m= 350$ GeV, $\varphi_o = H_I\lambda^{-1/4}$ and $\dot{\varphi}_o = H_I^2$. - The upper curve is for $\alpha = 10^{-3}$, the middle curve is for $\alpha = 10^{-2}$, the lower curve is for $\alpha = 5 \times 10^{-2}$. The particle creation processes are accounted for numerically [1].	60
6.5	The evolution of the baryon charge $B(\eta)$ for $\lambda_1 = 5 \times 10^{-2}$, $\lambda_2 = \lambda_3 = 5 \times 10^{-4}$, $\alpha = 10^{-3}$, $m= 350$ GeV, $\varphi_o = H_I\lambda^{-1/4}$ and $\dot{\varphi}_o = H_I^2$. - The upper curve is for $H = 10^9$ GeV, the middle curve is for $H = 10^{10}$ GeV, the lower curve is for $H = 10^{11}$ GeV. The particle creation processes are accounted for numerically [1].	61
6.6	The evolution of the baryon charge $B(\eta)$ for $\lambda_1 = 10^{-2}$, $\lambda_2 = \lambda_3 = 10^{-3}$, $\alpha = 10^{-2}$, $m=500$ GeV, $\varphi_o = H_I\lambda^{-1/4}$ and $\dot{\varphi}_o = H_I^2$	62
6.7	The evolution of the baryon charge $B(\eta)$ for $\lambda_1 = 5 \times 10^{-2}$, $\lambda_2 = \lambda_3 = 10^{-2}$, $\alpha = 5 \times 10^{-2}$, $H = 10^{11}$ GeV, $\varphi_o = H_I\lambda^{-1/4}$ and $\dot{\varphi}_o = H_I^2$. - The upper curve is for $m = 100$ GeV, the middle curve is for $m = 200$ GeV, the lower curve is for $m = 350$ GeV. The particle creation processes are accounted for numerically [1].	63
6.8	The evolution of the baryon charge $B(\eta)$ for $\lambda_1 = 10^{-2}$, $\lambda_2 = \lambda_3 = 10^{-3}$, $\alpha = 10^{-2}$, $H = 10^{11}$ GeV, $\varphi_o = H_I\lambda^{-1/4}$ and $\dot{\varphi}_o = H_I^2$	64
6.9	The evolution of the baryon charge $B(\eta)$ for $\alpha = 10^{-3}$, $m=350$ GeV, $H = 10^{12}$ GeV, $\lambda_{2,3} = 10^{-4}$, $\varphi_o = H_I\lambda^{-1/4}$ and $\dot{\varphi}_o = H_I^2$. - The upper curve is for $\lambda_1 = 10^{-3}$, the middle is for $\lambda_1 = 10^{-2}$ and the lower - for $\lambda_1 = 3 \times 10^{-2}$. The particle creation processes are accounted for numerically [2].	66

6.10 **The evolution of the baryon charge $B(\eta)$ for $\alpha = 10^{-3}$, $m=350$ GeV, $H = 10^{12}$ GeV, $\lambda_1 = 10^{-2}$, $\varphi_o = H_I \lambda^{-1/4}$ and $\dot{\varphi}_o = H_I^2$.** - The upper curve is for $\lambda_{2,3} = 10^{-4}$, the middle is for $\lambda_{2,3} = 10^{-3}$ and the lower - for $\lambda_{2,3} = 5 \times 10^{-3}$. The particle creation processes are accounted for numerically [2]. 67

List of Tables

1.1	Recent SBBN predictions of primordial light element abundances	11
1.2	Recent observational estimations and theoretical predictions of primordial ${}^4\text{He}$ production	18

Introduction

Background and motivation

According to the Standard model in Cosmology, the baryon content and the observed baryon asymmetry of the Universe were created after inflation, during a baryogenesis process. There exist observational data on baryon density and the baryon asymmetry of the Universe. There are precise measurements of the baryon density from different observational data, namely data based on the consistency between theoretically obtained and observationally measured abundances of the light elements produced in BBN [3], data based on the measurements of Deuterium towards low metallicity quasars combined with BBN data [4] and data based on the measurements of the CMB anisotropy [5]. Constraints from Cosmic Rays and Gamma Rays data show that locally (20 Mpc) the Universe is baryon-antibaryon asymmetric.

We still do not know how exactly baryogenesis has happened, i. e. the exact baryogenesis mechanism is not known. Moreover, it is yet not established if the baryon asymmetry is a local or a global characteristic of our Universe. Baryon number violation is a necessary condition to produce an observational excess of baryons over antibaryons. However, there is no experimental evidence of particle processes with significant B violation. Hence these issues are interesting and actual.

Many baryogenesis models exist, the most popular among which are Great Unified Theories baryogenesis [6], Electroweak baryogenesis [7], Baryo-through-lepto-genesis [8] and Affleck-Dine baryogenesis models [9]. In series of works of this thesis we construct and study a Scalar field condensate baryogenesis model, based on the Affleck and Dine baryogenesis scenario. This model is attractive because it is compatible with inflation and it evades the monopole and domain wall problems. In fact, in contrast to the other models, our scenario produces higher than observed today baryon asymmetry, which

can be reduced to the observed today value by particle creation mechanism. Also, the available observational data for the baryon density and CR and GR data can be used to constrain the particular baryogenesis model [10]. Another attractive feature of this type of the inhomogeneous SFC baryogenesis scenario is that it is able to produce matter and antimatter domains separated by large enough empty spaces, thus providing an option to create a matter-antimatter symmetric Universe in agreement with CR, GR and CMB observational constraints.

The construction of a successful baryogenesis model is also useful for constraining the parameters of the model, provided by physics theories, i. e. constrain physics beyond Standard model, like SUSY.

The chemical composition of the baryonic content of the observed Universe is another intriguing issue of the contemporary cosmology and astrophysics. The baryon component of our Universe is mainly Hydrogen and Helium, which were mainly produced during Big Bang Nucleosynthesis at early hot stage of the Universe evolution. In contrast to baryogenesis, nowadays we know precisely the processes of light elements formation, namely BBN.

BBN is used as the most precise test of beyond the Standard model physics. One of the interesting processes beyond SM are neutrino oscillations - when neutrino spontaneously changes its flavour during its propagation through space.

Present data coming from Cosmic Microwave Background and Large Scale Structures and BBN allow the existence of one extra sub-eV mass sterile neutrino (neutrino, which does not participate in weak interactions and couldn't be detected), additional to the well known three active neutrino species [11]. Furthermore sterile neutrino with mass in KeV region is a candidate for Warm Dark Matter [12].

Nowadays there are many experimental evidences for the existence of neutrino oscillations, provided by solar, atmospheric and terrestrial neutrino experiments. Some of the neutrino experiments also point to an existence of an additional light sterile neutrino [13]. Besides, a better fit to the solar problem with participation of a very light sterile neutrino has been proposed by [14]. Sterile neutrino, if presents, participates in neutrino oscillations and hence could be produced in neutrino oscillations. Thus, it is interesting to explore the cosmological influence of sterile oscillating neutrinos and the cosmological constraints on its parameters.

It is interesting how the neutrino oscillations effect BBN processes. It is well known that the flavour neutrino oscillations practically do not effect BBN. On the other hand active-sterile neutrino oscillations exert strong effect on BBN and especially on the primordial He-4 production [15]. The investigation of the effects of active-sterile neutrino oscillations on the BBN processes is important for studying physics beyond the Standard model.

Helium-4 is the most abundant in the Universe after Hydrogen and has simple post BBN evolution and, respectively, it is the most precisely calculated and measured element. Until 2010 it was believed the He-4 abundance is measured with 3% uncertainty, while theoretical uncertainty is less than 0.1% within a wide range of values of baryon to photon ratio. However, later it was found that the systematic errors had been underestimated and currently we know that there is a room for over 5% deviation from the mean value of the measured primordial He-4 abundance and the central value is larger than the one obtained before. We used this new observations as a base of our study of BBN with oscillations and obtained bounds on oscillation parameters for 5% He-4 overproduction.

Aims and objectives

Thus, our work is dedicated to two attractive themes in modern cosmology - baryogenesis and the chemical composition of the baryonic component in non-standard BBN with neutrino oscillations.

The first aim of our work is to construct BBN with electron-sterile neutrino oscillations. Our second aim is to study the effects of the neutrino oscillations on BBN processes. Further, our objective is to obtain isohelium countours of 5% He-4 overproduction for a range of oscillation parameters and different initial population of the sterile neutrino state.

Another aim of our work is to collect and discuss observational data of antimatter in cosmic and gamma rays, obtained from different balloon flights and spacecrafts, as well as observational data concerning baryon density; to construct a successful baryogenesis model, i. e. to investigate the dependence of the baryon charge on model parameters and try to construct successful baryogenesis model.

The next chapter is dedicated to studying non-standard BBN with neutrino oscillations. The available BBN theoretical and observational data are discussed. The neutrino properties and solar, atmospheric and accelerator experiments for its detection are presented. The model of nonequilibrium electron-sterile oscillations for the case when ν_s do not thermalize till $T = 2$ MeV and oscillations become effective after ν_e decoupling is introduced. The dynamical and kinetic effects of neutrino oscillations on BBN are discussed, as well as the production of neutrino-antineutrino asymmetry. BBN constraints on neutrino oscillation parameters for 5% He-4 overproduction and different initial population of the sterile state are obtained. They are compared with earlier obtained bounds for 3% He-4 overproduction and their behaviour is discussed.

In the second chapter baryogenesis and Scalar field baryogenesis scenario, in particular, are discussed. The baryon asymmetry and the baryon density of the Universe are discussed, as well as the most popular baryogenesis models. Our Scalar field baryogenesis model, based on the Affleck and Dine baryogenesis scenario, is introduced. The precise numerical analysis is provided and the role of particle creation processes is studied. Also, the dependence on different model parameters is studied. An inhomogeneous scalar field condensate baryogenesis model is discussed.

Part I

Processes important for the formation of the chemical content of the Universe

1

Big Bang Nucleosynthesis theory and observations

The theory of Hot Big Bang beginning of the Universe and synthesis of elements in its very early ages was first proposed by George Gamow and his collaborators Ralph Alpher and Robert Herman in 1946-1950 [16, 17]. Later the Big Bang Nucleosynthesis (BBN) theory was developed and now it is recognized as one of the greatest successes of the Standard Big Bang cosmology because of the remarkable agreement between the theoretical predictions and the observational abundances of the primordially produced elements. BBN occurred during the temperature range of approximately 1 MeV to 0.1 MeV, which corresponds to times of 1 to 200 sec, or the first three minutes of the life of our Universe, when four light elements were produced - D (^2H), ^3He , ^4He and ^7Li .

The Standard Model of BBN (SBBN) relies on General relativity to describe the evolution of the early Universe. The primordial abundances of the light elements in SBBN practically depends only on one parameter - baryon to photon ratio or baryon number density:

$$\eta = \frac{n_b}{n_\gamma} = \frac{(n_n + n_p)}{n_\gamma} \quad (1.1)$$

At present times, η is obtained independently through Cosmic Microwave Background radiation measurements with high precision. However, η_{CMB} corresponds to much later epoch $\sim 380\,000$ years. In case η has not changed between the two epochs, it becomes possible for SBBN theory to be verified.

In the very early Universe the temperature was so high that all matter constituents were fully ionized and dissociated. At the pre-BBN epoch the following weak interactions took place:

$$n \leftrightarrow p + e^- + \bar{\nu}_e \quad (1.2)$$

$$\begin{aligned} n + \nu_e &\leftrightarrow p + e^- \\ n + e^+ &\leftrightarrow p + \bar{\nu}_e \end{aligned} \quad (1.3)$$

At $T > 1MeV$ these weak interactions were in thermal equilibrium and fixed the ratio of neutron to proton number densities to be:

$$\frac{n}{p} = e^{-\frac{\Delta m}{T}}, \quad (1.4)$$

where $\Delta m = 1.293MeV$ is the neutron-proton mass difference.

The weak processes rate

$$\Gamma_{n \leftrightarrow p} = n \langle \sigma v \rangle \sim G_F^2 T^5 \quad (1.5)$$

(n is the number density of the relativistic electrons and positrons, σ and v are the cross section and velocity of the weak interactions and G_F is Fermi's coupling constant) was much higher than the Hubble expansion rate

$$H = \sqrt{\frac{8}{3}\pi G_N \rho} \sim \sqrt{g_* G_N} T^2 \quad (1.6)$$

(ρ is the energy density of the Universe, $g_* = (11/2) + (7/4)N_\nu$ is the number of relativistic particle species determining the energy density in radiation, N_ν is the neutrino number and G_N is Newton's gravitational constant) at this time. When the Universe cooled down, with dropping of the temperature T , $\Gamma_{n \leftrightarrow p}$ fell faster than H and at a time when $T \sim 0.7MeV$ they became comparable, the equilibrium was broken. The moment of so called "freeze out" occurs when $\Gamma_{n \leftrightarrow p} \sim H$ at freezing temperature

$$T_{fr} \sim \left(\frac{g_* G_N}{G_F^4} \right)^{1/6} \simeq 1MeV \quad (1.7)$$

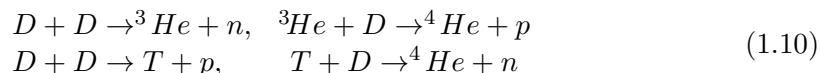
The neutron to proton ratio froze at a value

$$\left(\frac{n}{p}\right)_{fr} = e^{-\frac{\Delta m}{T_{fr}}} \simeq \frac{1}{6}. \quad (1.8)$$

Below T_{fr} the weak reactions 1.3 stop, the evolution of neutron-proton ratio is determined only by neutron β -decay with neutron mean life-time τ_n . The (n/p) drops to $\simeq 1/7$ since the time of nuclear reactions beginning. This simplified analytical approach gives $(n/p)_{fr}$ to an accuracy of $\sim 1\%$. After the freeze out of the neutron-proton interconverting processes, chains of nuclear reactions take place, which start with the formation of Deuterium D - an isotope of Hydrogen made of 1 proton and 1 neutron, with binding energy $B_D = m_n + m_p - m_D = 2.224MeV$

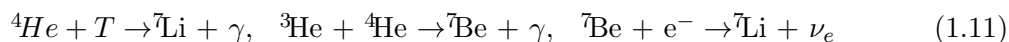


and then proceed in two possible chains



(T is Tritium - an isotope of H made of 1 proton and 2 neutrons).

During these reactions the protons and neutrons tend to form mainly Helium nuclei. In order to produce 4He , it is required first to form D. However, at the time of BBN, the temperature was still so high that the D nuclei were broken apart by high-energy gamma rays as soon as they formed. Therefore 4He production was suppressed until $T \simeq 0.1MeV$, effect known as Deuterium bottleneck. At $T < 0.1MeV$ extremely rapid element formation processes occur. Because of the two-body nuclear collisions, the probability of synthesis of havier elements increases with an increase of the baryon number density η and therefore less D survives with larger η . Thus, all surviving neutrons since BBN beginning end up bound in 4He . A small amount of Lithium - 7Li is produced through the following reactions:



Havier nuclei do not form in any significant quantity because η is too small and the three-body collisions do not occur.

The mass fraction of primordial ${}^4\text{He}$ is

$$Y_p = \frac{A_{He}n_{He}}{n_b}, \quad (1.12)$$

where $A_{He} = 4$ is Helium atomic mass. As we assume all neutrons are bound in ${}^4\text{He}$, then

$$Y_p \sim \frac{2 \left(\frac{n}{p}\right)_{fr} e\left(\frac{-t}{\tau_n}\right)}{1 + \left(\frac{n}{p}\right)_{fr}} \simeq 0.25 \quad (1.13)$$

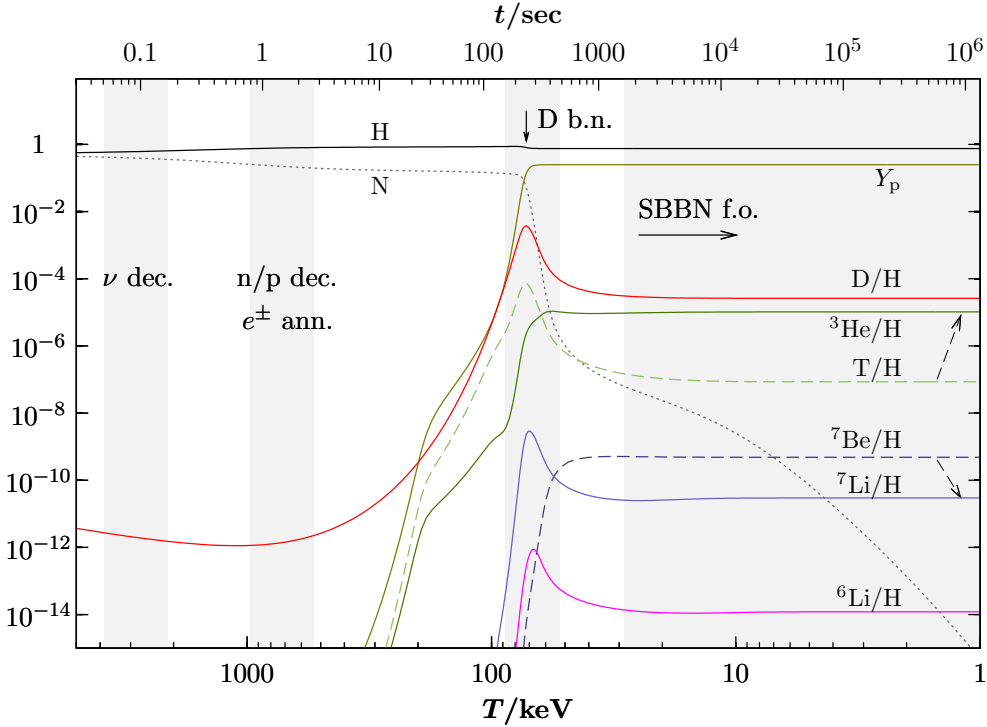


Figure 1.1: The evolution of primordial nuclei synthesis in SBBN model - The vertical bands present important BBN stages - ν decoupling, n/p freeze out, D bottleneck and nuclear reactions freeze out. Protons - H and neutrons - N are expressed relatively to baryon number and Y_p is ${}^4\text{He}$ mass fraction. The upward arrow marks off the time when most of the ${}^4\text{He}$ is produced and the downward one - the time when ${}^7\text{Be}$ went to ${}^7\text{Li}$ [18].

BBN stops shortly thereafter, at about 20 minutes after the Big Bang when our Universe becomes too cool for any nuclear reactions to proceed. The budget summary

1.1 Theoretical calculations of the primordial abundances of the light elements

of primordially produced light elements shows ${}^4\text{He} \sim 0.25$ by mass fraction, D and ${}^3\text{He}/H \sim$ few times of 10^{-5} and ${}^7\text{Li}/H \sim 10^{-10}$, for the range of $\eta = (1 - 10) \times 10^{-10}$. In Fig. 1.1 the time and temperature behaviour of light element abundances calculated in SBBN are illustrated. The evolution is shown through the main important stages of the primordial nucleosynthesis as ν decoupling from the thermal bath, $e^- - e^+$ annihilation and n/p freezing, Deuterium bottleneck and the drop out of equilibrium of all nuclear reactions.

1.1 Theoretical calculations of the primordial abundances of the light elements

Theoretical predictions of the light element primordial abundances depends on three main parameters in general - neutron mean life-time, which is determined with pretty good precision

$$\tau_n = 880.1 \pm 1.1s \quad [3], \quad (1.14)$$

the number of light neutrino species, which is

$$N_\nu = 3.046 \quad [19], \quad (1.15)$$

in the Standard Cosmological Model and the baryon to photon ratio from eq. 1.1, which is determined by WMAP (Wilkinson Microwave Anisotropy Probe) as

$$\eta = (6.19 \pm 0.14) \times 10^{-10} \quad [5, 20]. \quad (1.16)$$

These are used to make precise calculations of the primordial element abundances, which are used for comparison with the observationally obtained values. The first precise SBBN code was worked out by Wagoner and his collaborators in 1967 and since then many codes were developed to calculate the primordial nuclei abundances with high accuracy [21, 22, 23, 24, 25]. In Tabl. 1.1 we present two recent precisely calculated values of the primordial abundances of the light elements obtained in SBBN. As it could be seen the calculated values by different authors are in good agreement. Furthermore SBBN prediction for Y_p impresses with its precision compared to measured ones [see 1.2].

1.2 Observational values of the primordial abundances of the light elements

D/H	Y_p	${}^3\text{He}/\text{H}$	${}^7\text{Li}/\text{H}$
$(2.49 \pm 0.17) \times 10^{-5}$	0.2486 ± 0.0002	$(1.00 \pm 0.07) \times 10^{-5}$	$5.24_{-0.67}^{+0.71} \times 10^{-10}$
1.79×10^{-5}	0.250	0.903×10^{-5}	7.08×10^{-10}

Table 1.1: Recent SBBN predictions of primordial light element abundances for $\eta = (6.23 \pm 0.17) \times 10^{-10}$ for the first line [26] and $\eta \simeq 6.24 \times 10^{-10}$ for the second line [25].

1.2 Observational values of the primordial abundances of the light elements

The observational abundances of the primordial elements are derived from astrophysical observations of different objects in our Universe.

1.2.1 Deuterium

Deuterium has simple post BBN behaviour since it is only destroyed in nuclear burning in stars and chemical evolution in galaxies. Therefore its measured value anywhere in the Universe could be used as a lower limit of the primordial abundance. The most precise observational data for primordial D abundance are found in the spectra of 7 high redshift, low metallicity QSO Absorption Line Systems. The data obtained from these 7 QSOALS give

$$D/H = (2.82 \pm 0.21) \times 10^{-5} \quad [27]. \quad (1.17)$$

As could be seen in Fig. 1.2, the obtained data show large dispersion and, even more, no obvious correlation with redshift or metallicity. On the other hand it presents a good agreement to the theoretically predicted value.

1.2.2 Helium-3

In contrast to D, ${}^3\text{He}$ could be both produced and depleted in the course of galactic evolution. Therefore, a direct interpretation of the results from ${}^3\text{He}/\text{H}$ measurements is not possible. ${}^3\text{He}$ is observed in the Solar System and more preferably in the Galactic HII regions. As in the case of D, ${}^3\text{He}$ does not show correlation with metallicity or position in the Galaxy and the obtained data exhibit a large variation. In [28] an

1.2 Observational values of the primordial abundances of the light elements

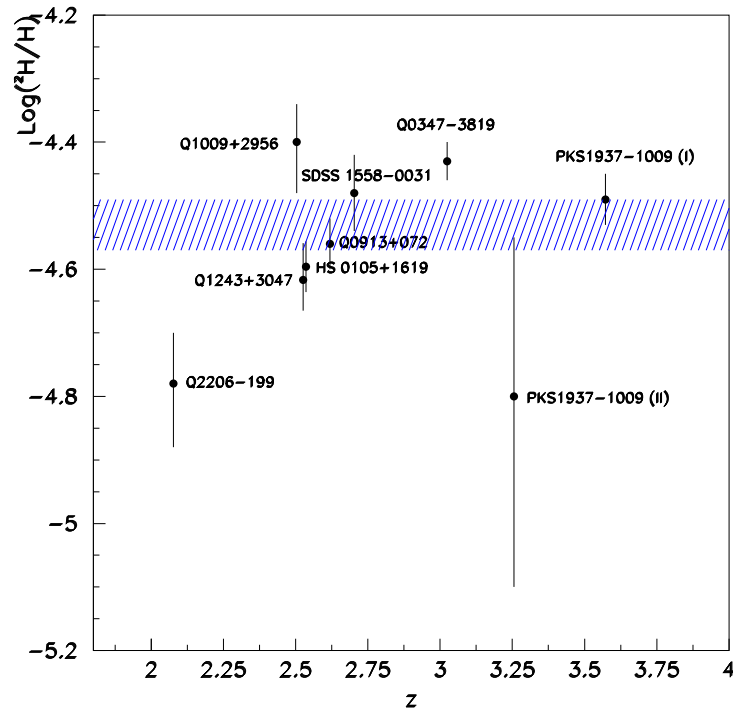


Figure 1.2: D/H ratios for different QSO systems as a function of the redshift
- The horizontal band presents the mean D/H ratio [25].

1.2 Observational values of the primordial abundances of the light elements

observational bound of ${}^3\text{He}/D < 1$ was obtained, which is in a good agreement with the SBBN predictions. Using observations of a peculiar galactic HII region the authors of [29] report upper limit of

$${}^3\text{He}/H < (1.1 \pm 0.2) \times 10^{-5}. \quad (1.18)$$

The comparison of the data with this upper bound is presented in Fig. 1.3.

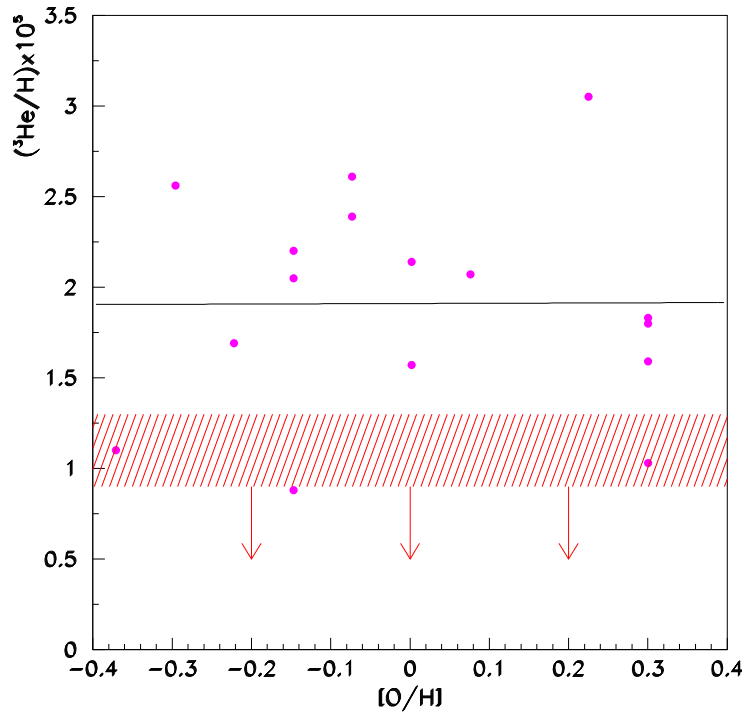


Figure 1.3: ${}^3\text{He}/H$ for observations with different metallicity - The solid line presents the linear fit of the data and the band is the upper limit on the primordially produced ${}^3\text{He}/H$ value obtained by these authors [29].

1.2.3 Lithium-7

The primordial abundance of Li is extracted from observations of metal poor stars in the spheroid of our Galaxy (Pop II), with metallicity up to 10^{-5} of the Solar metallicity value. Since Li shows a significant correlation with Fe its observational abundance is obtained by extrapolating to zero metallicity. There are several values of the primordial

1.2 Observational values of the primordial abundances of the light elements

Li obtained by different analysis and observations and the representative range which includes all of them gives

$$Li/H = (1.58 \pm 0.31) \times 10^{-10} \quad [30]. \quad (1.19)$$

The determination of primordial Li is made simultaneously on both ${}^6\text{Li}$ and ${}^7\text{Li}$ isotopes but ${}^7\text{Li}$ is the dominant one. In Fig. 1.4 a comparison of the SBBN predictions and the data for Li abundance, obtained for different observations as a function of metallicity, are presented. As could be seen none of the observationally obtained Li abundance is consistent with SBBN calculations. This is so called lithium problem.

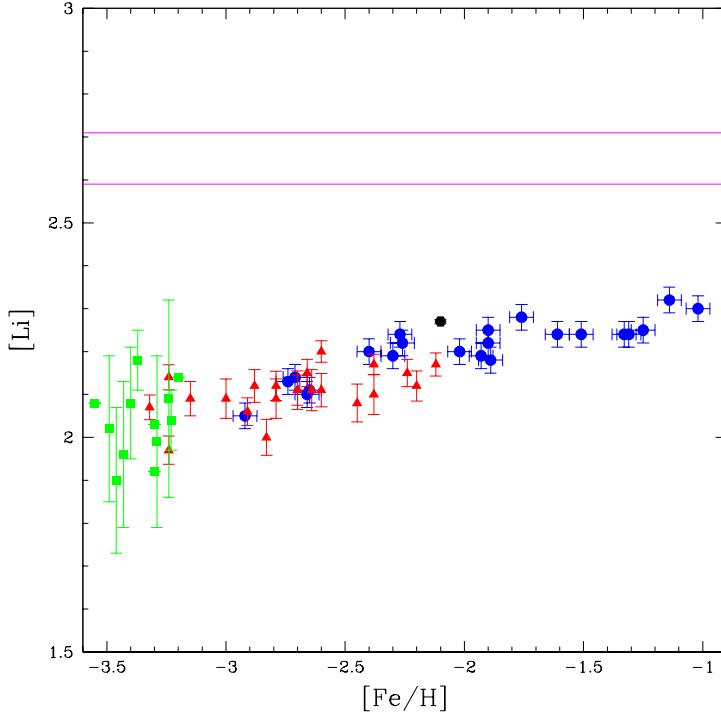


Figure 1.4: The Lithium abundance for different observational objects as a function of metallicity - The Li abundance is presented as $[Li]=12+\log(Li/H)$ and the metallicity is given by Fe/H . The band shows SBBN prediction for Li within the range $\pm 1\sigma$ [31].

1.2 Observational values of the primordial abundances of the light elements

1.2.4 Helium-4

The post BBN behaviour of ${}^4\text{He}$ is simple as it is only produced in the stellar and galactic chemical evolution. The ${}^4\text{He}$ is most abundant (after H), most precisely calculated and measured element. The observations of ${}^4\text{He}$ are made using H and He recombination lines from low metallicity extragalactic HII regions, like compact blue dwarf galaxies. The linear correlaton between ${}^4\text{He}$, produced in stars (Y) and metals Z (C, N and O) is used to derive the primordial mass fraction Y_p .

$$Y = Y_p + Z \left(\frac{dY}{dZ} \right), \quad \text{when } Z \rightarrow 0, \quad Y \rightarrow Y_p \quad (1.20)$$

The most recent observationally derived abundances of Y_p are present in Tabl. 1.2 where one can see the impressive accuracy of the values obtained. The very good consistancy with the theoretically predicted primordial abundances is evident. For illustration in Fig. 1.5 the linear fit of Y_p versus O/H relation for all data of authors in [32] is presented.

In Fig. 1.6 the calculated abundances of light elements as a function of η are presented. As could be seen, the primordial abundance of ${}^4\text{He}$ slowly rises with η , because at larger η the processes of BBN start earlier and less neutrons decay till then. On the contrary D abundance quickly drops down when rising η because of the tendency for synthesis of the heavier and more tightly bound nuclei - ${}^4\text{He}$. This tendency becomes larger with increasing of the baryon number density, therefore less D survives at larger η . Since D is extremely sensitive to the value of η it could be used as a "baryometer" to probe the cosmological baryon density. For all the light elements the systematic errors are the main limitation to reach the necessary precision of the observationally received primordial abundances. The minimization of these errors may help to overcome the problem of inconsistency of some of the observational abundances in comparison with theoretically predicted ones. However, the unresolved puzzles of SBBN may point also to a Physics beyond the Standard Model, for example additional neutrino species.

Primordially produced ${}^4\text{He}$ is the preferred light element for obtaining limits on non-standard physics, because its post BBN evolution is simple since it is only produced in stars. Also nowadays ${}^4\text{He}$ is calculated and measured with remarkable precision. The thoretical predictions of the most abundant light element have impressive accuracy of more than 1%. In Tabl. 1.2 some recent theoretical estimations of the primordial ${}^4\text{He}$

1.2 Observational values of the primordial abundances of the light elements

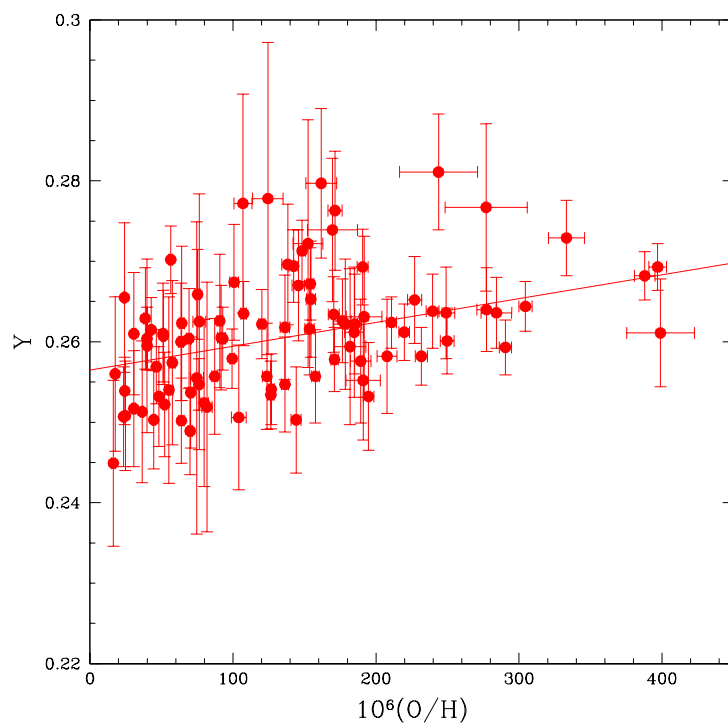


Figure 1.5: The derivation of the primordial ${}^4\text{He}$ mass fraction - Y is obtained using the linear fit of all data obtained from 96 spectra in 86 HII regions and then extrapolated to zero metallicity [32].

1.2 Observational values of the primordial abundances of the light elements

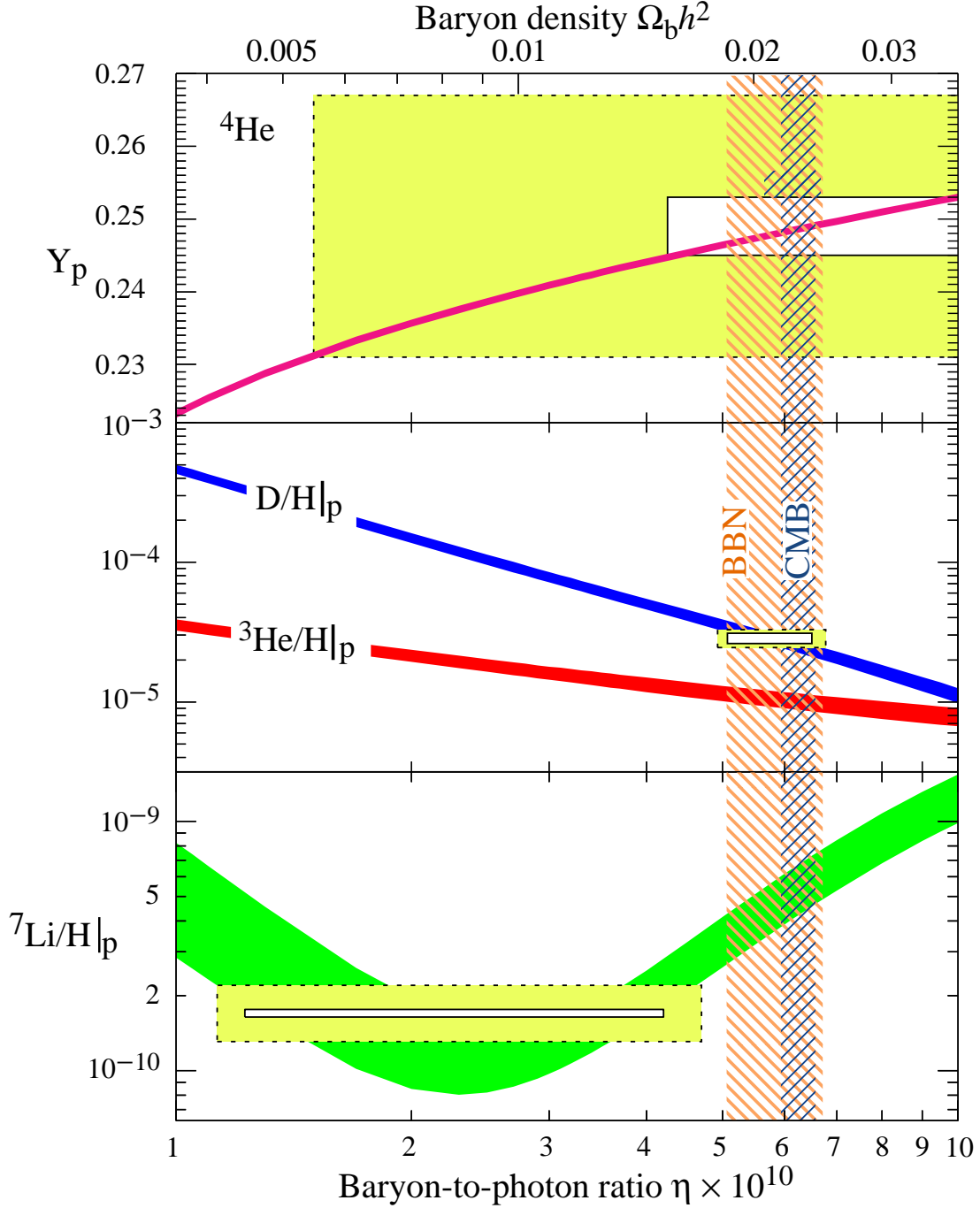


Figure 1.6: The abundances of light elements predicted by the SBBN model with 95%*C.L.* (wide bands) as a function of baryon to photon ratio η - The narrow vertical band presents CMB measure of η and the wide one indicates the BBN concordance range, both with 95%*C.L.* Smaller boxes show observed element abundances with $\pm 2\sigma$ statistical error, while larger ones present $\pm 2\sigma$ statistical + systematic error [32].

1.2 Observational values of the primordial abundances of the light elements

mass fraction Y_p are collected and presented [33]. Determinations from astrophysical observations in metal poor HII regions are given for comparison. The high level of consistency of the theoretical and observational results is evident. More careful analysis of the data points to a higher central value of the observed Y_p compared to the theoretical predictions with only several percent uncertainty, which makes actual the interpretation of ${}^4\text{He}$ overproduction

$$\frac{\delta Y_p}{Y_p} \geq 5\% \quad (1.21)$$

as due to mechanisms beyond standard physics. Such an appropriate mechanism could be additional light ν species, active to sterile neutrino oscillations [34, 35, 36, 37], etc.

$Y_p(\text{theor})$	References	$Y_p(\text{obs})$	References
0.2486 ± 0.0002	[26]	$0.2565 \pm 0.0010(\text{stat.}) \pm 0.0050(\text{syst.})$	[32]
0.2482 ± 0.0007	[38]	$0.2561 \pm 0.0108(\text{stat.} + \text{syst.})$	[39]
0.2479 ± 0.0002	[40]	$0.2573 \pm 0.0033(\text{stat.} + \text{syst.})$	[41]
		$0.250 \pm 0.003(\text{stat.} + \text{syst.})$	[25]

Table 1.2: Recent observational estimations and theoretical predictions of primordial ${}^4\text{He}$ production [33]

In this subsection we described the processes of light elements formation in the early Universe, which are strongly dependent on neutrino particle properties. We showed that ${}^4\text{He}$ is the most abundant element, measured and calculated with remarkable precision. Current observational data for its abundance point to an effective number of neutrino flavours $N_\nu > 3$ higher than predicted by the Standard Model of Particle physics [19]. Also, we showed that the systematic uncertainty in ${}^4\text{He}$ measurements points to a discussion of helium overproduction higher than 5%.

2

Neutrino and neutrino oscillations

Neutrino played very important role in the BBN processes in the early Universe. For the first time neutrino was postulated in 1930 by Wolfgang Pauli for explanation of β -decay: $n^0 \rightarrow p^+ + e^- + \bar{\nu}_e$. The first detection was provided by Cowan, Reines, Harrison, Kruse and McGuire in 1956 [42] and brought them the Nobel Prize later in 1995. The name of the particle was given by Enrico Fermi, who further developed the theory of β -decay.

Within the Standard Model, where the base of matter are 6 quarks and 6 leptons, we know that the neutrino is an electrically neutral lepton, which interacts through the weak and gravitational forces. It is a massless elementary particle with a half-integer spin $1/2\hbar$, i.e. it is a fermion. Three flavours of neutrino are known - electron neutrino - ν_e , muon neutrino - ν_μ and tau neutrino - ν_τ and their anti particles - $\bar{\nu}_e$, $\bar{\nu}_\mu$ and $\bar{\nu}_\tau$.

2.1 Neutrino oscillations detection

2.1.1 Solar neutrino anomaly

The first attempts to detect and measure neutrinos produced in the Sun were made by Raymond Davis and Jr. and John N. Bahcall in the early 50s and later in 1968 they started an experiment in a golden mine of Homestake, South Dakota, USA [43, 44]. A tank with $380 m^3$ of perchloroethylene was placed 1478 m underground, where upon collision with a neutrino, a chlorine atom was transformed into a radioactive isotope of

2.1 Neutrino oscillations detection

argon and then was extracted and counted. This way it was possible to determine how many neutrinos have been captured. The solar neutrino production, penetrating through layers of different density and thickness from the core to the surface, and propagation through space to reach the Earth are well known and the expected solar neutrino flux can be precisely calculated. In the Homestake experiment, however, the detected electron neutrinos were about 1/3 of the theoretically predicted and the discrepancy in results essentially created the solar neutrino anomaly.

In 1957 Bruno Pontecorvo developed the idea for neutrino oscillations [45]. The idea was based on the non-zero mass of neutrino and distinguishes between neutrino mass eigenstates - ν_1, ν_2, ν_3 and flavour eigenstates - ν_e, ν_μ, ν_τ . Then each mass eigenstate could be presented as a superposition of the flavour eigenstates (and vice versa) and therefore when propagates neutrino can switch between different flavours. Thus for example, if electron neutrino flux travels through space, after a time, a part of the flux could be composed by muon and tau neutrinos. Thus the neutrino physics goes beyond the Standard Model where neutrino is a massive particle.

After the Homestake experiment many scientists around the world were working on the solar neutrino problem, like Kamiokande in Japan [46], SAGE [47] in the former Soviet Union, GALLEX and GNO in Italy [48, 49], Super Kamiokande [50]. All these experiments confirmed the solar neutrino deficit and showed that it depends on the energy of the neutrino.

Finally, in 2001, scientists working at SNO, the Sudbury Neutrino Observatory in Ontario, Canada, found strong evidence that the neutrino oscillates [51, 52]. SNO was a 1000 tonnes heavy water (D_2O) Cherenkov detector designed to detect neutrinos produced by fusion reactions in the Sun, built about 2 km under ground, in Creighton mine, Sudbury, Canada. In it neutrinos reacted with the heavy water to produce Cherenkov radiation and this light was then detected by an array of 9600 photomultiplier tubes. SNO was able to detect all types of neutrinos coming from the Sun and to distinguish between electron neutrinos and the other two flavors. It found that about 35% of the arriving solar neutrinos are electron neutrinos, with the others being muon or tau neutrinos. The total number of detected neutrinos agrees quite well with the theoretical predictions.

2.1.2 Atmospheric neutrino anomaly

Another very important aspect of the neutrino properties investigation is the resolving of the atmospheric neutrino anomaly. An isotropic cosmic ray flux from protons and heavy nuclei enter the Earth's atmosphere continuously. As a result of the interactions in the atmosphere pions and kaons are produced which decay and produce electron and muon neutrinos with different energies. For the energies less than 1 GeV the theoretical predictions give ratio $r \sim \nu_e/\nu_\mu = 2$. Also due to the spherical symmetry of the atmosphere and the isotropy of the cosmic rays flux an identical up- and down-coming fluxes are expected. However, the underground neutrino experiments like IMB [53], Super Kamiokande [54], Soudan 2 [55] and Macro [56] measured considerably lower than expected r and observed a dependence of the muon neutrino deficit on the neutrino energy and the zenith angle. These data were explained by $\nu_\mu \leftrightarrow \nu_\tau$ neutrino oscillations.

2.1.3 Accelerator neutrino experiments

Strong evidences for oscillations of muon neutrinos were obtained also in the long-baseline accelerator neutrino experiments K2K [57] and MINOS [58]. In addition, a short-baseline accelerator experiment LSND observed a possible indication for $\bar{\nu}_\mu \rightarrow \bar{\nu}_e$ oscillations [59]. However, in the MiniBooNE experiment no indications of $\nu_\mu \rightarrow \nu_e$ oscillations were found yet [60, 61].

Briefly, data from atmospheric and long baseline oscillation experiments may be explained well by muon to tau neutrino oscillations. Similarly, solar and reactor neutrino data are explained well by electron to muon or electron to tau neutrino oscillations. However, the results from LSND and MiniBooNE may point to the extension to the Standard Model including models with an additional or even more than one light sterile neutrinos.

2.2 Sterile neutrino

The measurement of the number of neutrino types comes from the observation of the Z boson decay into any light neutrino (light here means neutrinos with mass less than a half of the Z boson mass) and its antineutrino, since the lifetime of Z boson is shorter if

more flavours of light neutrinos are available. Recent detections provided in [62] show the following number of flavours of light neutrino:

$$N_\nu = 2.984 \pm 0.008 \quad (2.1)$$

However, beyond the Standard Model there is a possibility of an existence of relatively light sterile neutrinos ν_s , which do not participate in the weak interactions and therefore could not be detected in Z boson decay processes. These sterile neutrinos could be produced in neutrino oscillations.

The neutrino oscillations data from LSND and MiniBooNE suggest existence of 1 or even 2 light sterile neutrinos with masses in the 1 eV range, which participate into oscillations with the flavour ones [63, 64].

Observations of neutrino oscillations imply that the masses of the neutrinos involved cannot be equal to one another and therefore they cannot both be zero.

The relation between flavour and mass eigenstates could be expressed through a unitary matrix U, called Pontecorvo-Maki-Nakagawa-Sakata or PMNS Matrix [45, 65]

$$\nu_m = U_{mf} \nu_f, f = (e, \mu, \tau). \quad (2.2)$$

For two oscillating neutrinos the PMNS Matrix is presented by 2×2 matrix:

$$U = \begin{bmatrix} \cos \theta & \sin \theta \\ -\sin \theta & \cos \theta \end{bmatrix}$$

Therefore

$$\begin{aligned} \nu_1 &= c\nu_i + s\nu_j \\ \nu_2 &= -s\nu_i + c\nu_j, \end{aligned} \quad (2.4)$$

where $s = \sin \theta$, $c = \cos \theta$, ν_1 and ν_2 are mass eigenstates and ν_i and ν_j are the flavour ones. Parameter θ is one of the neutrino oscillation parameters, called mixing angle.

In the two particle case, when propagating, neutrino changes its type with probability:

$$P_{i \rightarrow j, i \neq j} = \sin^2 2\theta \sin^2 \left(\frac{\delta m^2 L}{4E} \right), \quad (2.5)$$

where L is oscillation distances, E - neutrino energies and δm^2 is the second neutrino oscillations parameter, named squared mass difference.

2.3 Neutrino oscillations parameters

The angles θ_{21} and $\theta_{31}(\theta_{23})$ are identified respectively as "solar" and "atmospheric" mixing angles, while δm_{21}^2 and $\delta m_{32}^2(\delta m_{31}^2)$ respectively as "solar" and "atmospheric" neutrino mass squared differences.

The best fit values ($\pm 1\sigma$) of the 3-neutrino oscillation parameters, derived from a global fit of the current neutrino oscillations data results from [66] give:

$$\begin{aligned} \delta m_{21}^2 &= 7.58_{-0.26}^{+0.22} \times 10^{-5} eV^2, & \sin^2 \theta_{12} &= 0.306(0.312)_{-0.015}^{+0.018} \\ |\delta m_{31}^2| &= 2.35_{-0.09}^{+0.12} \times 10^{-3} eV^2, & \sin^2 \theta_{23} &= 0.42_{-0.03}^{+0.08} \end{aligned} \quad (2.6)$$

The existing data do not allow to determine the sign of $\delta m_{31(32)}^2$.

Recently θ_{13} was measured by Daya Bay experiment [67]:

$$\sin^2 2\theta_{13} = 0.089 \pm 0.010(stat.) \pm 0.005(syst.) \quad (2.7)$$

At Fig. 2.1 we present a plot of δm^2 as a function of $\tan 2\theta$, which shows the regions inside the lines that are excluded by various experiments with 90% C.L.

As a conclusion, in this subsection we reviewed the strong evidences that neutrinos oscillate. Also, we point to the indications for existence of a sterile neutrino, which does not participate in ordinary weak interactions and therefore is hard to detect.

2.4 Specifications of the BBN with electron-sterile neutrino oscillations model

The aim of our work is to study the effects of active-sterile neutrino oscillations on Big Bang Nucleosynthesis and to obtain cosmological bounds on neutrino oscillation

2.4 Specifications of the BBN with electron-sterile neutrino oscillations model

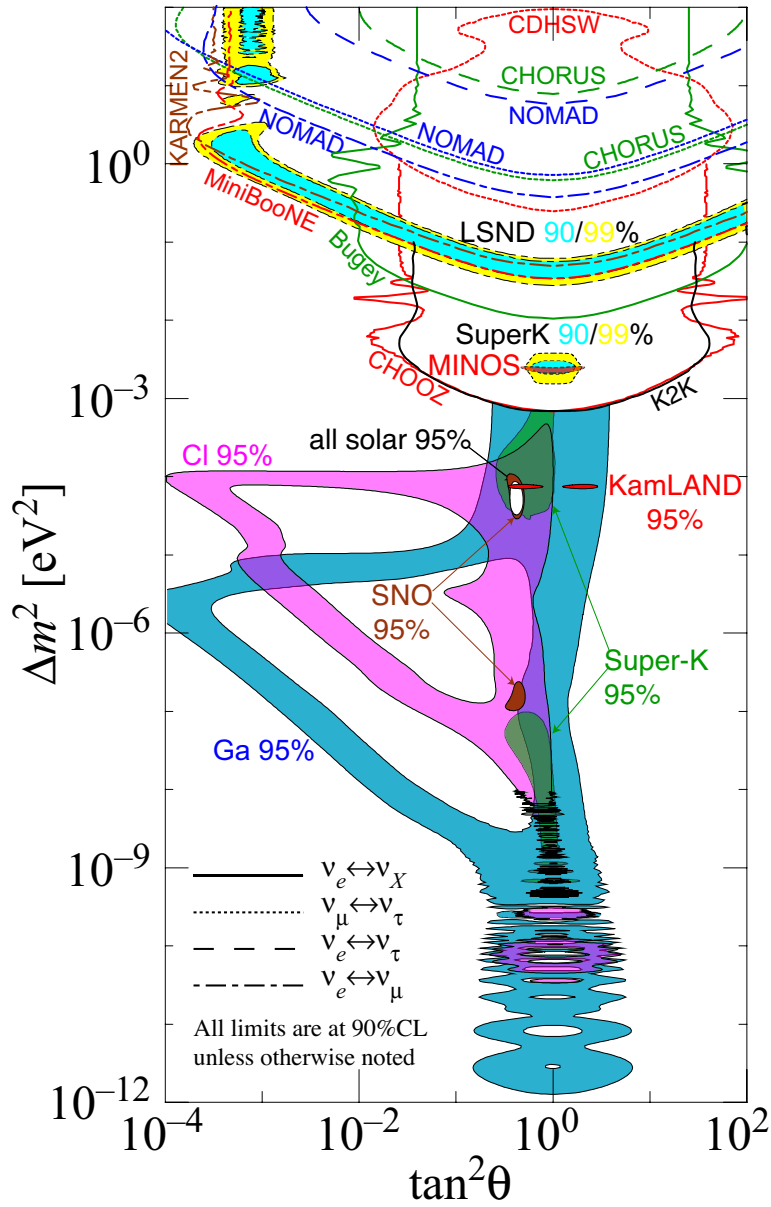


Figure 2.1: Oscillation parameter δm^2 as a function of $\tan^2 \theta$ - Regions inside the lines are excluded by various experiments with 90% C.L. [3].

2.4 Specifications of the BBN with electron-sterile neutrino oscillations model

parameters. We discuss nonequilibrium oscillations between weak interacting electron neutrinos ν_e and sterile neutrinos ν_s for the case when ν_s do not thermalize till $T = 2$ MeV and oscillations become effective after ν_e decoupling. Basic characteristics of our model are [68]:

1. We examine **oscillations between the sterile ν_s and the active ν_e** , according to the Majorana-Dirac mixing scheme [69]. For simplicity, we have chosen two particle case - **mixing only in the electron sector** (see 2.4).

$$\begin{aligned}\nu_1 &= c\nu_e + s\nu_s \\ \nu_2 &= -s\nu_e + c\nu_s,\end{aligned}\tag{2.8}$$

where ν_s denotes the sterile electron antineutrino, $s = \sin\theta$, $c = \cos\theta$, θ is the mixing angle in the electron sector, the mass eigenstates ν_1 and ν_2 are Majorana particles with masses correspondingly m_1 and m_2 . The flavour neutrino oscillations have negligible effect on the neutrino number densities and on BBN because of the very slight deviation from equilibrium in that case [15] and therefore the assumption of two mixing case is acceptable.

2. Since the sterile neutrinos do not participate in the ordinary weak interactions, we consider that they **decouple much earlier than the active ones**. After ν_s decoupling, active neutrinos, which are still in equilibrium, have been additionally heated due to annihilation and decays of particles. Thus in later epochs the temperature and number densities of ν_s are considerably less than those of ν_e .
3. If $\nu_e \leftrightarrow \nu_s$ oscillations are allowed, sterile neutrinos may not decouple earlier enough in comparison with the active ones and their nonequilibrium densities may not be considerably different. They may come to thermal equilibrium again if already decoupled [70]. The reactions of ν_e with the plasma are the source of thermalization for ν_s , because when oscillating into active neutrinos they may interact with the medium and thus thermalize. That is why, in order to assure a nonequilibrium case, we assume also that **neutrino oscillations become effective after the decoupling of the active neutrinos**, $\Gamma_{osc} \geq H$ for $T \leq 2MeV$. This constraints the neutrino mass difference:

$$\delta m^2 \leq 1.3 \times 10^{-7} eV^2 \quad [68]\tag{2.9}$$

2.4 Specifications of the BBN with electron-sterile neutrino oscillations model

4. The last assumption of our model is that **sterile neutrinos should not thermalize till 2 MeV when oscillations become effective**, so the production rate of ν_s must be smaller than the expansion rate. This gives limits on the allowed range of oscillation parameters:

$$\sin^2(2\theta)\delta m^2 \leq 10^{-7} eV^2 \quad [68] \quad (2.10)$$

In our work, we provide precise numerical analysis of the evolution of nonequilibrium oscillating neutrinos integrating the kinetic equations for the neutrino density matrix in momentum space for the period after the electron neutrino decoupling till the neutron-proton ratio freezing, i.e. for $T = [2 - 0.3 MeV]$. The rates of expansion of the Universe, neutrino oscillations and neutrino interactions with the medium are comparable in our model, that is why we use kinetic equations which account simultaneously for the participation of neutrinos into those three processes. In our analysis we consider both resonant $\delta m^2 = m_2^2 - m_1^2 < 0$ and nonresonant $\delta m^2 > 0$ neutrino oscillations. The range of oscillation parameters studied is $\delta m^2 = [10^{-10} - 10^{-7}] eV^2$ and $\theta = [0 - \pi/4]$.

In the epoch before BBN the Universe was consisting of plasma of photons, neutrinos, electrons, and small quantities of nucleons. The kinetic equations for the density matrix of the nonequilibrium oscillating neutrinos in that epoch have the form [35, 68]:

$$\frac{\partial \rho(t)}{\partial t} = Hp \frac{\partial \rho(t)}{\partial p} + i [\mathcal{H}_o, \rho(t)] + i [\mathcal{H}_{int}, \rho(t)] + O(\mathcal{H}_{int}^2), \quad (2.11)$$

where p is the momentum of electron neutrino and ρ is the density matrix of the massive Majorana neutrinos in momentum space.

The first term in the equation describes the effect of expansion, the second describes the oscillations and the third - for neutrino scattering of the medium. The free neutrino hamiltonian \mathcal{H}_o is:

$$\mathcal{H}_o = \begin{pmatrix} \sqrt{p^2 + m_1^2} & 0 \\ 0 & \sqrt{p^2 + m_2^2} \end{pmatrix}, \quad (2.12)$$

$\mathcal{H}_{int} = \alpha V$ is the interaction hamiltonian, where $\alpha_{ij} = U_{ie}^* U_{je}$, $V = G_F (\pm L - Q/M_W^2)$. It plays the role of induced squared mass for electron neutrinos:

$$\mathcal{H}_{int}^{LR} = \begin{pmatrix} V & 0 \\ 0 & 0 \end{pmatrix}. \quad (2.13)$$

2.4 Specifications of the BBN with electron-sterile neutrino oscillations model

The first term in V accounts for charged-current and neutral-current interactions with protons, neutrons, electrons and positrons, neutrinos and antineutrinos from the medium and is proportional to the fermion asymmetry of the plasma $L = \sum_f L_f$, which is assumed of the order of the baryon asymmetry.

$$L_f \sim \frac{N_f - N_{\bar{f}}}{N_\gamma} T^3 \sim \frac{N_B - N_{\bar{B}}}{N_\gamma} T^3 = \beta T^3. \quad (2.14)$$

The second term in V arises as an W/Z propagator effect, $Q \sim E_\nu T^4$. For the early epochs of the Universe life both terms must be accounted for because they both are significant.

The last term in the Eq. 2.11 describes the weak interactions of neutrinos with the medium. For example, for the weak reactions of neutrinos with electrons and positrons $e^+e^- \leftrightarrow \nu_i \tilde{\nu}_j$, $e^\pm \nu_j \rightarrow e'^\pm \nu'_i$ it has the form:

$$\begin{aligned} & \int d\Omega(\tilde{\nu}, e^+, e^-) \left[n_{e^-} n_{e^+} \mathcal{A} \mathcal{A}^\dagger - \frac{1}{2} \{ \rho, \mathcal{A}^\dagger \bar{\rho} \mathcal{A} \}_+ \right] \\ & + \int d\Omega(e^-, \nu', e'^-) \left[n'_{e^-} \mathcal{B} \rho' \mathcal{B}^\dagger - \frac{1}{2} \{ \mathcal{B}^\dagger \mathcal{B}, \rho \}_+ n_{e^-} \right] \\ & + \int d\Omega(e^+, \nu', e'^+) \left[n'_{e^+} \mathcal{C} \rho' \mathcal{C}^\dagger - \frac{1}{2} \{ \mathcal{C}^\dagger \mathcal{C}, \rho \}_+ n_{e^+} \right], \end{aligned} \quad (2.15)$$

where n is the number density of the interacting particles, \mathcal{A} is the amplitude of the process $e^+e^- \rightarrow \nu_i \tilde{\nu}_j$, \mathcal{B} is the amplitude of the process $e^- \nu_j \rightarrow e'^- \nu'_i$ and \mathcal{C} - of the process $e^+ \nu_j \rightarrow e'^+ \nu'_i$. They are expressed through the known amplitudes $\mathcal{A}_e(e^+e^- \rightarrow \nu_e \tilde{\nu}_e)$, $\mathcal{B}_e(e^- \nu_e \rightarrow e^- \nu_e)$ and $\mathcal{C}_e(e^+ \nu_e \rightarrow e^+ \nu_e)$:

$$\mathcal{A} = \alpha \mathcal{A}_e, \quad \mathcal{B} = \alpha \mathcal{B}_e, \quad \mathcal{C} = \alpha \mathcal{C}_e \quad (2.16)$$

The neutrino kinetics down to 2 MeV is the same as in the standard case, since the electron neutrinos maintain their equilibrium distribution and the sterile ones are absent. Then the last term in the kinetic equation can be neglected and the equation results into couple of nonlinear integro-differential equations for the components of the density matrix.

The kinetic equation describing the evolution of the neutron number density in momentum space n_n with neutrino oscillations $\nu_e \leftrightarrow \nu_s$ has the form:

$$\begin{aligned} \frac{\partial n_n}{\partial t} = H p_n \frac{\partial n_n}{\partial p_n} & + \int d\Omega(e^-, p, \nu) |\mathcal{A}(e^- p \rightarrow \nu n)|^2 (n_{e^-} n_p - n_n \rho_{LL}) \\ & - \int d\Omega(e^+, p, \tilde{\nu}) |\mathcal{A}(e^+ n \rightarrow p \tilde{\nu})|^2 (n_{e^+} n_n - n_p \bar{\rho}_{LL}). \end{aligned} \quad (2.17)$$

2.4 Specifications of the BBN with electron-sterile neutrino oscillations model

The first term accounts for the expansion of the Universe and the second one for the processes: $e^- + p \leftrightarrow n + \nu_e$ and $p + \tilde{\nu}_e \leftrightarrow e^+ + n$, which directly influence the nucleon density. Number densities per unit volume are expressed as $N = (2\pi)^{-3} \int d^3p n(p)$. The neutrino and antineutrino density matrices may be different, $\bar{\rho}_{LL} \neq \rho_{LL}$, compared to the standard case. Therefore, the term differs from the standard scenario by the substitution of ρ_{LL} and $\bar{\rho}_{LL}$ instead of $n_\nu^{eq} \sim \exp(-E_\nu/T)/1 + e^{E_\nu/T}$.

Fig. 2.2 illustrates the difference in nuclear freezing in different cases: Standard BBN case without oscillations, the vacuum oscillation case and the scenario with matter neutrino oscillations.

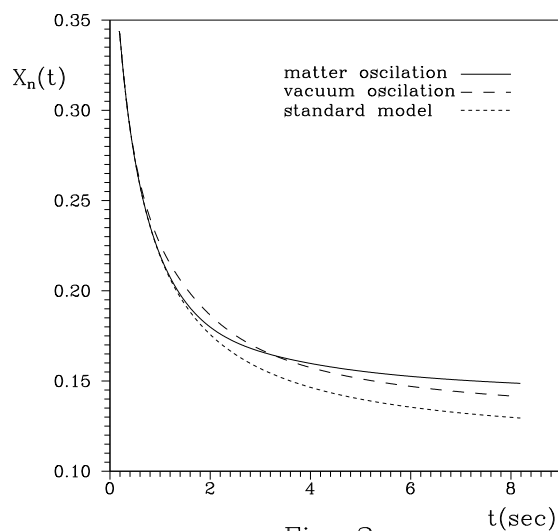


Fig. 2

Figure 2.2: The illustration of nonequilibrium neutrino oscillations effects on BBN. - The behaviour of neutrons to nucleons freezing ratio $X_n = n_n^f/n_{nuc}$ with time is presented for the three scenarios - Standard BBN without oscillations, BBN with vacuum oscillations and BBN with matter neutrino oscillations [68].

In this subsection we discussed our model's features and main assumptions. Here we described the kinetic equations for the neutrino density matrix in momentum space. We provided precise numerical analysis of the evolution of nonequilibrium oscillating neutrinos integrating these equations for the period after the ν_e decoupling until the n/p -freezing.

2.5 Cosmological effects of neutrino oscillations

Contrary to the flavour neutrino oscillations which effect BBN negligibly, active-sterile neutrino oscillations can exert strong effect on BBN and particularly primordial ${}^4\text{He}$ production. As far as $\nu_e \leftrightarrow \nu_s$ neutrino oscillations can fill the initially empty or partially filled sterile state, $0 \leq \delta N_s < 1$, they lead to an increase of the effective number of neutrino species $N_{eff} = 3 - \delta N_s$ and the relativistic degrees of freedom during BBN $g_* = 10.75 + 7/4\delta N_s$. This speeds up the expansion of the Universe, $H(t) \sim g_*^{1/2}$ (see 1.6, 1.7, 1.8, 1.13), causes earlier n/p-freezing, at times when neutrons are more abundant and, hence, leads to overproduction of ${}^4\text{He}$ [34, 71]. This *Dynamical effect* gives up to 5% ${}^4\text{He}$ overproduction when one additional neutrino type is brought into equilibrium by oscillations.

The *Kinetic effect* of oscillations may be much stronger than $\delta N_s = 1$ in case of oscillations effective after ν decoupling, proceeding between partially populated sterile neutrino state $0 \leq \delta N_s < 1$ and electron neutrino [35, 68, 72, 73]. The non-equilibrium initial condition, for most of the oscillations parameters of the model, leads to considerable and continuous deviations from the equilibrium ν_e spectrum (spectrum distortion) because the oscillation rate depends on energy according to $\Gamma \sim \delta m^2/E$. The distortion leads to both a depletion of the active neutrino number density and a decrease of the Γ . Thus it influences the nucleon kinetics, causing an earlier n/p -freezing and an overproduction of ${}^4\text{He}$ yield. The spectrum distortion is the greatest, if the sterile state is empty at the beginning of oscillations, $\delta N_s = 0$. It decreases with the increase of the degree of population of the sterile state at the onset of oscillations [74] as illustrated in the Fig. 2.3.

Besides this leading kinetic effect of oscillations there is known an additional subdominant effect, namely the *Production of neutrino-antineutrino asymmetry*. Neutrino-antineutrino asymmetry may be generated during the resonant transfer of neutrinos [72, 75]. This dynamically produced asymmetry suppresses oscillations at small mixing angles, leading to less overproduction of He-4 compared to the case without the account of asymmetry growth, and hence alleviating BBN constraints on oscillation parameters.

The presence of non-zero initial sterile neutrino population influences BBN as follows: first, it increases the expansion rate and then in the $\nu_e \leftrightarrow \nu_s$ oscillations case, the presence of ν_s at the onset of oscillations influences the kinetic effects of $\nu_e \leftrightarrow \nu_s$

2.5 Cosmological effects of neutrino oscillations

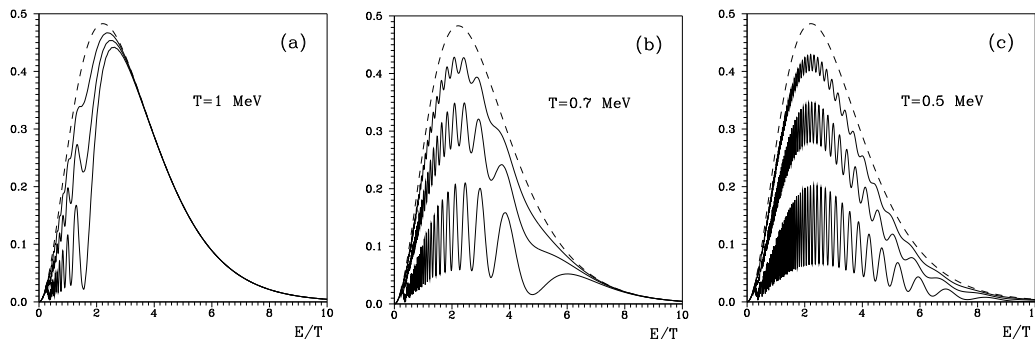


Figure 2.3: The spectrum distortion at different degrees of population of the steriles

- $\delta N_s = 0$ (lower curve), $\delta N_s = 0.5$ and $\delta N_s = 0.8$ (upper curve). The dashed curve gives the equilibrium spectrum for comparison. It is obvious that the distortion of the spectrum is considerable and with time, involves the whole neutrino ensemble [74].

on BBN. Larger δN_s decreases the kinetic effects, because the element of initial non-equilibrium between the active and the sterile states is less expressed [76].

Neutrino spectrum distortion effect is very strong even when there is a considerable population of the sterile neutrino state before the beginning of the electron-sterile oscillations. The kinetic effects are the strongest for $\delta N_s = 0$, they disappear for $\delta N_s = 1$, when ν_e and ν_s states are in equilibrium, and the total effect reduces to the SBBN with an additional neutrino. The cosmological constraints on oscillations parameters for the case of $\delta N_s \neq 0$ are changed.

The total effect can be approximately described by $\delta Y_p \sim 0.013\delta N$, where $\delta N = \delta N_s + \delta N_{kin}$, $\delta N_{kin} = \delta N_{kin}^{max}(1 - \delta N_s)$ and δN_{kin}^{max} is the kinetic oscillations effect, corresponding to $\delta N_s = 0$. The expression presents a good approximation to the numerically calculated dependence of the kinetic effect on the initial population of ν_s , derived in reference [74].

2.5.1 Dependence of Y_p on $\delta N_s \neq 0$ for the case, when $\delta Y_p/Y_p > 5\%$

There is an interesting interplay between the different effects which $\delta N_s \neq 0$ exerts on oscillations and on BBN models with oscillations and hence, the δY_p production and the cosmological constraints on oscillations parameters for the case $\delta N_s \neq 0$ differ from the ones derived before [78, 79, 80] for $\delta N_s = 0$.

2.5 Cosmological effects of neutrino oscillations

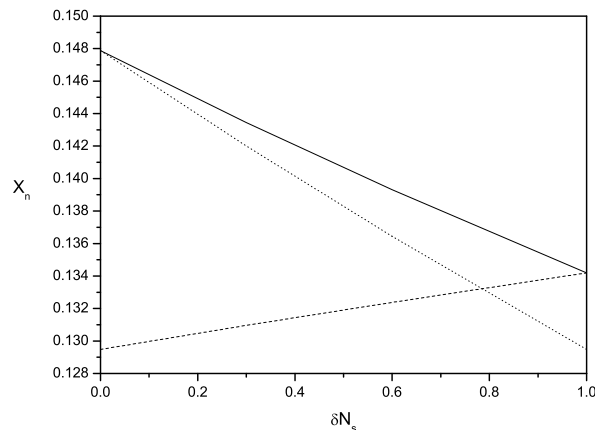


Figure 2.4: The dependence of the dynamical, kinetic and the total effect on δN_s value - The solid curve presents the frozen neutron density relative to nucleons $X_n = n_n^f/n_{nuc}$ as a function of the sterile neutrino initial population, at $\delta m = 10^{-7}$ eV² and $\sin^2 2\theta = 1$. The dotted curve presents the kinetic effect, while the dashed curve presents energy density increase effect [77].

As found in [81], for $\delta Y_p/Y_p > 5\%$ corresponding to $\delta N_{kin}^{max} > 1$, the suppression effect dominates over the dynamical effect of $\delta N_s \neq 0$. Hence, the total effect is a decreasing function of δN_s , i.e. ⁴He overproduction decreases with δN_s from its maximal value at $\delta N_s = 0$, and correspondingly, the BBN constraints on oscillation parameters relax.

In the opposite case $\delta Y_p/Y_p < 5\%$, corresponding to $\delta N_{kin}^{max} < 1$, the dynamical effect dominates and the total effect is increasing with δN_s . I.e. ⁴He overproduction increases and the BBN constraints on oscillations strengthen with δN_s . In the case $\delta Y_p/Y_p = 5\%$ the constraints for $\delta N_s \neq 0$ coincide with the ones for $\delta N_s = 0$, due to the cancellation of the two effects.

For illustration of $\delta N_{kin}^{max} > 1$ case, which we consider further on, we present in Fig. 2.4 the two effects on ⁴He overproduction at $\delta m = 10^{-7}$ eV² and $\sin^2 2\theta = 1$. We have studied numerically the contribution of these effects on neutrons to nucleons freezing ratio $X_n = n_n^f/n_{nuc}$ for different δN_s . The primordial yield of helium to a good approximation is expressed through X_n : $Y_p \sim X_n \exp(-t/\tau_n)$, where τ_n is the neutron lifetime. For the chosen set of parameters $\delta N_{kin}^{max} > 1$ and so the ⁴He overproduction decreases with the increase of δN_s . The suppression effect of δN_s dominates and a

2.5 Cosmological effects of neutrino oscillations

relaxation of the cosmological constraints compared to $\delta N_s = 0$ must be expected.

Briefly, here we discussed the effects which active-sterile neutrino oscillations exert on primordial ${}^4\text{He}$ production. We showed how the dynamical effect leads to ${}^4\text{He}$ overproduction through speeding up the Universe expansion. The kinetic effect also leads to overproduction through spectrum distortion of the equilibrium ν_e spectrum. An additional subdominant effect of production of neutrino-antineutrino asymmetry leads to less overproduction of ${}^4\text{He}$. Therefore, in order to derive bounds from BBN on neutrino oscillation parameters, it is necessary to account for the interplay of all effects.

3

BBN bounds on neutrino oscillations parameters

In our work we study BBN bounds on neutrino active-sterile oscillations, providing a numerical analysis of the BBN production of He-4, Y_p , in the presence of $\nu_e \leftrightarrow \nu_s$ oscillations and obtaining iso-helium contours, corresponding to different levels of He-4 overproduction, $\delta Y_p/Y_p$. We investigate cosmological bounds on oscillation parameters in two different cases - with initially empty sterile state $\delta N_s = 0$ and with initially partially filled sterile state $\delta N_s \neq 0$.

3.1 The case with empty initial population of the sterile neutrino, $\delta N_s = 0$

For $\delta N_s = 0$, the combined iso-helium contours for the nonresonant and the resonant case and different levels of helium overproduction, were calculated in refs. [78, 79, 80], accounting for all oscillations effects on BBN. These cosmological constraints, corresponding to $\delta Y_p/Y_p = 3\%$, excluded almost completely LOW (low probability or low mass) solution to the solar neutrino problem, besides the LMA (Large Mixing Angle) solution and sterile atmospheric solution, excluded in previous works. This result is consistent with the following global analysis of the neutrino experiments data, which do not favor $\nu_e \leftrightarrow \nu_s$ solutions as dominant solutions to Solar neutrino problem.

The analytical fits to the exact constraints for $\delta N_s = 0$ and $\delta Y_p/Y_p = 3\%$ were

3.2 The case with non-zero initial population of the sterile neutrino, $\delta N_s \neq 0$

calculated in [82]:

$$\begin{aligned} \delta m^2 (\sin^2 2\theta)^4 &\leq 1.5 \times 10^{-9} \text{eV}^2 \text{ for } \delta m^2 > 0 \\ |\delta m^2| &< 8.2 \times 10^{-10} \text{eV}^2 \text{ for } \delta m^2 < 0 \text{ and large } \theta \end{aligned} \quad (3.1)$$

However, recently it was found that there exists larger uncertainty in ${}^4\text{He}$ than believed before [32, 41]. And in our works [77, 83, 84, 85] we calculated isohelium contours for 5% ${}^4\text{He}$ uncertainty.

For $\delta N_s = 0$ and $\delta Y_p/Y_p = 5\%$ the analytical fits to the exact constraints are [33]:

$$\begin{aligned} \delta m^2 (\sin^2 2\theta)^7 &\leq 3.1 \times 10^{-9} \text{eV}^2 \text{ for } \delta m^2 < 0 \text{ and} \\ |\delta m^2| &< 1.7 \times 10^{-9} \text{eV}^2 \text{ for } \delta m^2 > 0 \text{ and large } \theta \end{aligned} \quad (3.2)$$

3.2 The case with non-zero initial population of the sterile neutrino, $\delta N_s \neq 0$

$\delta N_s \neq 0$ present before $\nu_{\mu,\tau} \leftrightarrow \nu_s$ just leads to an increase of the total energy density of the Universe, and it is straightforward to re-scale the existing constraints. In the $\nu_e \leftrightarrow \nu_s$ oscillations case, however, the presence of ν_s at the onset of oscillations influences in addition the kinetic effects of $\nu_e \leftrightarrow \nu_s$ on BBN. Hence a precise study of the cosmological constraints for that case is needed.

BBN constraints corresponding to $\delta Y_p/Y_p = 3\%$ overproduction of ${}^4\text{He}$ and non-zero initial population of the sterile neutrino $\delta N_s < 0.54$ were calculated in refs. [81, 86]. As far as $\delta Y_p/Y_p = 3\%$ corresponds to $\delta N_{kin}^{max} < 1$, the constraints strengthen with the increase of the sterile state population δN_s . They increase the BBN 3% ${}^4\text{He}$ exclusion region for oscillation parameters corresponding to $\delta N_s = 0$ towards smaller δm^2 .

Hence, having in mind the still-existing observational uncertainty of ${}^4\text{He}$ measurements and especially the existence of a large systematic error indicated by the existence of the different ${}^4\text{He}$ measurements, in our work [77] we provide a detail numerical calculation of cosmological constraints corresponding to $\delta Y_p/Y_p > 5.2\%$ ${}^4\text{He}$ overproduction ($\delta N_{kin}^{max} > 1$) and different initial degrees of sterile neutrino population in the range $0 \leq \delta N_s < 1$. We have chosen $\delta Y_p/Y_p = 5.2\%$, i.e. a value slightly higher than the critical one 5%, in order to illustrate the possibility for relaxation of the cosmological constraints on oscillations for $\delta N_s \neq 0$.

3.2 The case with non-zero initial population of the sterile neutrino, $\delta N_s \neq 0$

As one can see in Fig. 3.1, we have found that the cosmological constraints relax for 5.2% ${}^4\text{He}$ overproduction in comparison with 3% ${}^4\text{He}$ overproduction [33]. Our numerical analysis has shown that up to $\delta N_s = 0.5$ the cosmological constraints corresponding to 5.2% He overproduction are slightly relaxed and remain almost stringent, as before. However, the constraints can be considerably relaxed for higher δN_s values. And, as can be expected, the constraints vanish for $\delta N_s = 1$, as far as in that case the sterile state is full and the kinetic effect due to neutrino spectrum distortion disappears. In Fig. 3.1 $\delta Y_p/Y_p = 5.2\%$ BBN constraints are presented for different values of the initial population of the sterile state, namely the lowest dashed contour corresponds to a zero population $\delta N_s = 0$, the solid curve corresponds to $\delta N_s = 0.5$, the dotted and the dot dashed contours to $\delta N_s = 0.7$ and to $\delta N_s = 0.9$, respectively.

Up to $\delta N_s = 0.5$ the cosmological constraints are slightly relaxed in comparison with the case $\delta N_s = 0$, however, for higher δN_s values, the constraints relax noticeably. It should be noted that there are considerable constraints even for a very high δN_s values for that really high ${}^4\text{He}$ uncertainty. So the constraints on neutrino mixing parameter vanish only when the sterile state is in equilibrium before oscillations, i.e. $\delta N_s = 1$, when the kinetic effect due to neutrino spectrum distortion disappears.

The reason for the relaxation of the constraints is the predominance of the suppression of the oscillations kinetic effects over the dynamical effect for the given uncertainty of ${}^4\text{He}$.

All cosmological constraints corresponding to $\delta Y_p/Y_p > 5\%$ will have such behavior, namely, they will be relaxed in comparison to the constraints for $\delta N_s = 0$. And vice versa, the constraints corresponding to lower than 5% ${}^4\text{He}$ uncertainty will be more stringent than the ones for initially empty sterile neutrino state.

We have calculated cosmological constraints corresponding to $\delta N_s = 0.5$ initial population of the sterile neutrino and for different levels of helium overproduction [83].

Our numerical analysis has shown that up to $\delta N_s = 0.5$ the cosmological constraints corresponding to 3% and 5% He overproduction are slightly changed and remain stringent, as before in agreement with results found in ref. [74]. Hence, even for partially filled sterile state the cosmological constraints give the most stringent limit on oscillation parameters.

The cosmological constraints in the case of non-empty initially sterile state exclude almost completely LOW solution to the solar neutrino problem as well as the LMA

3.2 The case with non-zero initial population of the sterile neutrino, $\delta N_s \neq 0$

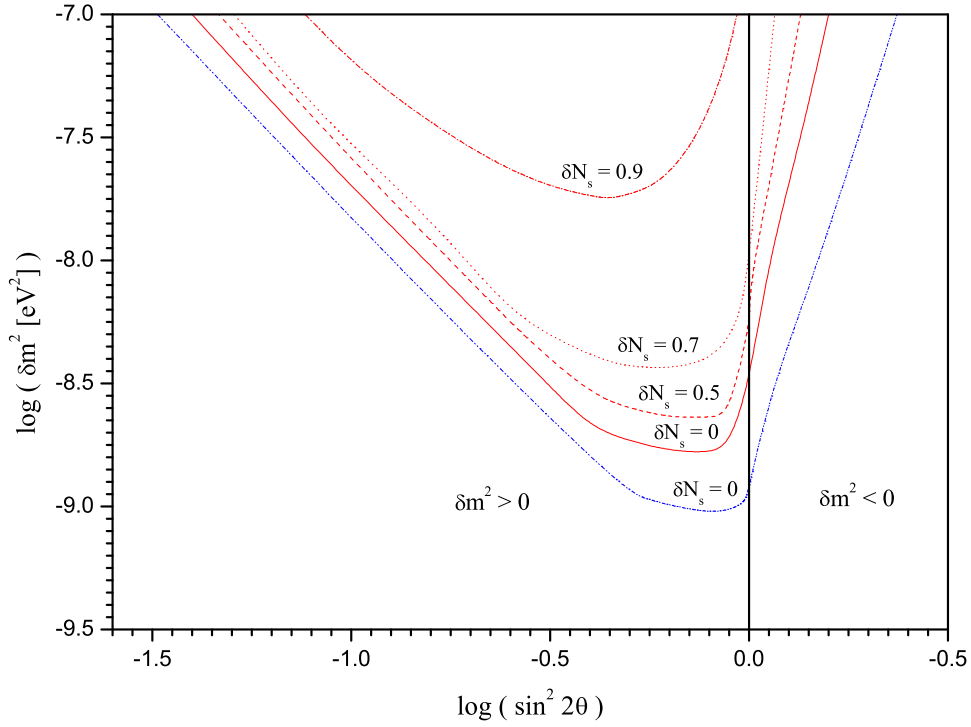


Figure 3.1: BBN constraints for $\delta Y_p/Y_p = 5.2\%$ and different δN_s values - The dashed contour presents $\delta Y_p/Y_p = 5.2\%$ BBN constraints for $\delta N_s = 0$, the solid curve corresponds to $\delta N_s = 0.5$, the dotted and the dot dashed contours - $\delta N_s = 0.7$ and to $\delta N_s = 0.9$, respectively. The case for $\delta Y_p/Y_p = 3\%$ and $\delta N_s = 0$ (the lowest curve) is presented for comparison. The resonant oscillations case corresponds to l.h.s of the figure, the non-resonant one to the r.h.s. [33, 77].

3.3 Discussion and conclusions

solution and sterile atmospheric solution. They are in agreement with the analysis of the experimental data from the solar and terrestrial neutrino oscillation experiments. Besides, the cosmological constraints are more restrictive by several orders of magnitude concerning the neutrino squared mass differences in comparison with the existing experimental constraints from neutrino oscillation experiments.

In Fig. 3.2 we present 5.2% helium-4 overproduction contours in comparison with the 3% ones (calculated in [81]) for two different cases, namely initially empty sterile state $\delta N_s = 0$ (dashed contours) and $\delta N_s = 0.5$ (solid contours), correspondingly. The two upper curves present 5.2% helium-4 overproduction, while the two lower curves give 3% helium-4 overproduction limits. As illustrated, non-zero initial population of the sterile neutrino leads to upwards shift of the helium 5.2% contour, on the contrary to the case of 3% helium contour, for which there is a downwards shift.

In summary, here we presented our results in deriving BBN bounds on neutrino oscillations parameters for ${}^4\text{He}$ overproduction of $> 5\%$. We calculated iso-helium contours for different initial populations of the sterile neutrino state and compared them with the ones for $\delta Y_p/Y_p = 3\%$. Also, we discussed the constraints behaviour in the context of neutrino oscillations effects on BBN.

3.3 Discussion and conclusions

We have studied BBN constraints on neutrino electron-sterile oscillations for the specific case when the sterile neutrino is partially filled initially. We have provided numerical analysis of the BBN production of ${}^4\text{He}$, Y_p , in the presence of electron-to-sterile neutrino oscillations, effective after electron neutrino decoupling. An account of all known oscillations effects on cosmological nucleosynthesis was made. We have calculated iso-helium contours corresponding to ${}^4\text{He}$ overproduction, $\delta Y_p/Y_p = 5\%$, for non-zero initial population of the sterile state $0 < \delta N_s < 1$. So, we have obtained the $\delta Y_p/Y_p = 5\%$ cosmological constraints on oscillation parameters corresponding to different δN_s values. The cosmological constraints for the cases $\delta N_s \leq 0.5$ are slightly changed in comparison to $\delta N_s = 0$ case. I.e. even in case the sterile state was initially non-empty within that range, the cosmological constraints on oscillation parameters remain the most stringent ones. However, for bigger δN_s the constraints are relaxed considerably and for $\delta N_s = 1$ they are alleviated.

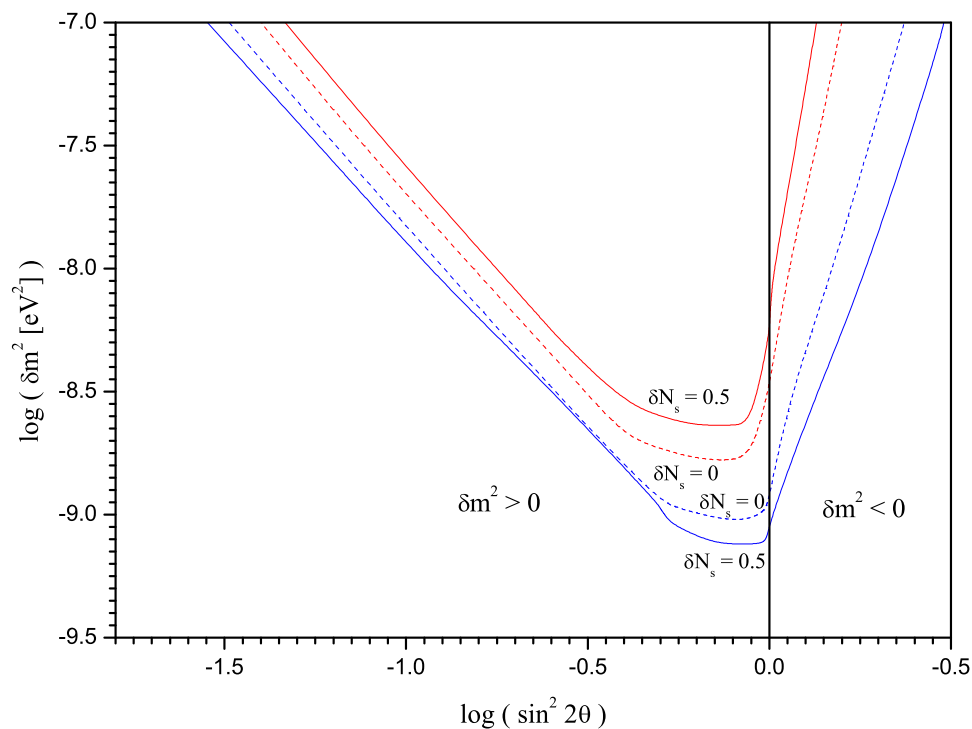


Figure 3.2: BBN constraints for $\delta Y_p/Y_p = 3\%$ and $\delta Y_p/Y_p = 5.2\%$ - The upper two contours present $\delta Y_p/Y_p = 5.2\%$ BBN constraints, while the lower two ones correspond to $\delta Y_p/Y_p = 3\%$. The dashed curves correspond to $\delta N_s = 0$ case, while the solid curves correspond to $\delta N_s = 0.5$. The resonant oscillations case is given to l.h.s of the figure, the non-resonant one to the r.h.s. [83]

3.3 Discussion and conclusions

The results are important for revealing neutrino properties, and are useful for defining the role of the sterile neutrino in the solar and atmospheric neutrino anomalies, as well as for constraining different models predicting the presence of sterile neutrinos in the early Universe.

These cosmological constraints are obtained for the case of 2-neutrino mixing and provide a comparison with the available 2-neutrino constraints for $\delta N_s = 0$ case. However at present, there exist strong evidence for flavor oscillations from solar, atmospheric and terrestrial neutrino oscillations experiments. Further generalization of the cosmological constraints on nonequilibrium electron-sterile neutrino oscillations both for the $\delta N_s = 0$ and for the $\delta N_s \neq 0$ case should include flavor neutrino mixing as well.

Qualitatively, for 4-neutrino or 5-neutrino mixing, the non-equilibrium initial population of the sterile state will cause spectrum distortion not only to electron neutrino but also to the other flavor neutrinos. Flavor neutrino oscillations with the parameters fixed from the solar and atmospheric neutrino data, will tend to reestablish the equilibrium between the different flavors. Hence, flavor mixing will partially compensate the distortion in the electron neutrino sector, caused by $\nu_e \leftrightarrow \nu_s$ oscillations, because the distortion will be redistributed among the 4 (or 5) neutrinos and hence electron neutrino state will be partially refilled (compared with the 2-neutrino case) for the sake of other flavor neutrinos. Consequently the kinetic effect of 4-neutrino oscillations on BBN will be reduced compared to 2-neutrino case $\delta N_{kin,4\nu(5\nu)}^{max} < \delta N_{kin,2\nu}^{max}$.

Correspondingly, the cosmological constraints on oscillation parameters in 4 or 5-neutrino mixing case will be less stringent than the ones calculated for 2-neutrino model. However, the shift of the constraints due to non-zero δN_s will keep its direction and remain proportional to δN_s , as in 2-neutrino case, but its value: $\delta N_{kin,4\nu}^{max} \times \delta N_s + \delta N_s$ will be reduced.

We have studied BBN constraints on neutrino $\nu_e \leftrightarrow \nu_s$ oscillations for the specific case when the sterile neutrino is partially filled initially $0 < \delta N_s < 1$. Non-zero δN_s has two-fold effect on BBN with neutrino oscillations: a dynamical effect leading to overproduction of He-4 and a kinetic effect, leading to underproduction of He-4 in comparison with the case of $\delta N_s = 0$. So, depending on the interplay between these opposite effects, the cosmological constraints may be either relaxed or strengthened.

Resuming the δN_s effect on BBN: Cosmological constraints corresponding to higher uncertainty of helium-4 than the one corresponding to one additional neutrino type

relax with the increase of the initial population of the sterile state, while the constraints corresponding to lower than that uncertainty of helium-4 strengthen with δN_s .

It is remarkable, that in case of BBN with non-equilibrium oscillations between electron and sterile neutrinos after neutrino decoupling, cosmological constraints on oscillation parameters exist even in the case when the ${}^4\text{He}$ abundance is known with uncertainty greater than 5%. Actually, it is possible to derive constraints on neutrino oscillation parameters for He-4 uncertainty up to 32% in the resonant oscillations case, and up to 14% uncertainty in the nonresonant oscillations case, as far as these are the maximal possible helium overproduction values [73]. The cosmological constraints persist while initially the sterile state is non equilibrium.

3.4 Future work

We have derived the constraints discussed above in a 2-neutrino mixing scheme. The account of flavor mixing, for which strong experimental evidence exists, will lead to a reduction of the spectrum distortion of the electron neutrino and hence, to a reduction of its kinetic effect on BBN. Consequently, the BBN constraints on oscillation parameters in 4-neutrino oscillation models will be relaxed in comparison with the 2-neutrino constraints discussed here. However, it is interesting to calculate numerically the case with flavour mixing and derive constraints from BBN on oscillation parameters, accounting for all types neutrino oscillations.

In our current work we consider the lepton asymmetry value L of order of the baryon asymmetry one B , as it is usually assumed. Cosmic neutrino background has not been measured yet and hence L is constrained only indirectly through its effects on BBN, CMB and LSS. The relic neutrino background may reveal L orders of magnitude bigger than the baryon one. Therefore, another aspect of our future work will be to provide our numerical analysis assuming $L > B$ and discuss the bounds on neutrino oscillation parameters from BBN in this case.

In our analysis we have used only primordial He-4 abundance to derive bounds from BBN on neutrino oscillations parameters. However, during BBN four light elements were produced - D (${}^2\text{H}$), ${}^3\text{He}$, ${}^4\text{He}$ and ${}^7\text{Li}$. The observational data for ${}^3\text{He}$ exhibit a large variation and the observationally obtained Li abundance is not consistent enough with the theoretical predictions to be used for obtaining constraints. On the other hand, at

present the observational data for primordial D abundance, obtained from observations of low metallicity QSO Absorption Line Systems, become more precise than in the past and are in a good agreement with the Standard BBN calculations. Hence, in future it is interesting to obtain BBN constraints on neutrino oscillations parameters, accounting for the primordial Deuterium abundance, as well.

Part II

Processes important for the generation of the baryonic content of the Universe

4

Baryon asymmetry of the Universe

A basic issue in cosmology is related to the content of our Universe. Currently observational data are provided from CMB by WMAP [5] and Planck [87] projects. According to these data nowadays the Universe contains $\sim 4 - 5\%$ baryons, $\sim 23\%$ dark matter and $\sim 72 - 73\%$ dark energy (the new data from Planck shows a little bit higher dark matter amount at the expense of the dark energy one).

The processes of formation of the baryonic content of the Universe and the observed baryon asymmetry are the subject of the Baryogenesis section in this work.

One of the amazing and still unresolved mysteries of our Universe is the fact that in our surroundings matter strongly dominates over antimatter. The baryon asymmetry β in our neighborhood within radius of 1 Mpc, indicated by cosmic and gamma rays observations, is:

$$\beta = \frac{n_B - n_{\bar{B}}}{n_\gamma} \sim \frac{n_B}{n_\gamma} = \eta, \quad (4.1)$$

where n_B is the baryon number density, $n_{\bar{B}}$ - antibaryon number density, n_γ - photon number density and η is the baryon density.

4.1 Cosmic and Gamma rays indications for matter domination in the Universe

Experimental search for *antinuclei and antiprotons* (\bar{p}) in *Cosmic Rays (CR)* were conducted on high-altitude balloons (see for example BESS, CAPRICE, MASS) and on

4.1 Cosmic and Gamma rays indications for matter domination in the Universe

spacecrafts (PAMELA, AMS-01, AMS-02). Antiprotons \bar{p} detected in primary cosmic radiation over energies 0.1 – 19 GeV are with negligible numbers, their ratio to protons consists few 10^{-5} for energies lower than 2 GeV and a few 10^{-4} for higher energies [88]. They can be totally explained as secondaries from interactions of primary CR particles with the interstellar medium.

In Fig. 4.1 we present all the published BESS (Balloon-borne Experiment with Superconducting Spectrometer) high-altitude balloon data [89, 90, 91, 92, 93], namely the antiproton spectrum for 1995, 1997-2000. As far as the measurements of \bar{p} spectrum at energies above a few GeV are free of uncertainties due to secondary \bar{p} production and solar modulation effects, we present also CAPRICE (Cosmic AntiParticle Ring Imaging Cherenkov Experiment) [94] and MASS (Matter Antimatter Spectrometer) [95] \bar{p} high energy measurements. The curves present the theoretical predictions for the secondary \bar{p} by Bieber J. [96] and Bergstrom L., et. al. [97], calculated within contemporary two-zone diffusion models for the corresponding level of solar activity. The uncertainties due to propagation range between 10% and 20% depending on the part of the spectrum [98].

Although the measured \bar{p} -flux and its spectrum is in agreement with the predicted ones for secondary particles, the data do not exclude a primary component.

In conclusion, the statistical sample of \bar{p} presently available is very limited, so that a primary component cannot be ruled out with high significance, even in case the propagation parameters were known. Besides, CR at the rigidities accessible to current antimatter experiments should be strongly suppressed by galactic, cluster and intergalactic magnetic fields [89].

No antinuclei has been observed in CR yet. The search for antihelium and anti-carbon continue in missions of AMS-02 (Alpha Magnetic Spectrometer) and PAMELA (Payload for Antimatter Matter Exploration and Light-nuclei Astrophysics) as far as their detection would be a certain signature for antimatter BBN or antistar, because the secondary flux for nuclei is expected to be extremely low [100]. By not detecting any antihelium, the AMS-01 established an upper limit of 1.1×10^{-6} for the antihelium to helium flux ratio [101]. PAMELA mission searches with sensitivity of 4.7×10^{-7} [102]. AMS-02 will reach a sensitivity of 10^{-9} , three orders of magnitude better than AMS-01, hugely extending the volume of the Universe which can be tested for the existence of primordial antimatter [103]. Recently, the first results from AMS-2 has been

4.1 Cosmic and Gamma rays indications for matter domination in the Universe

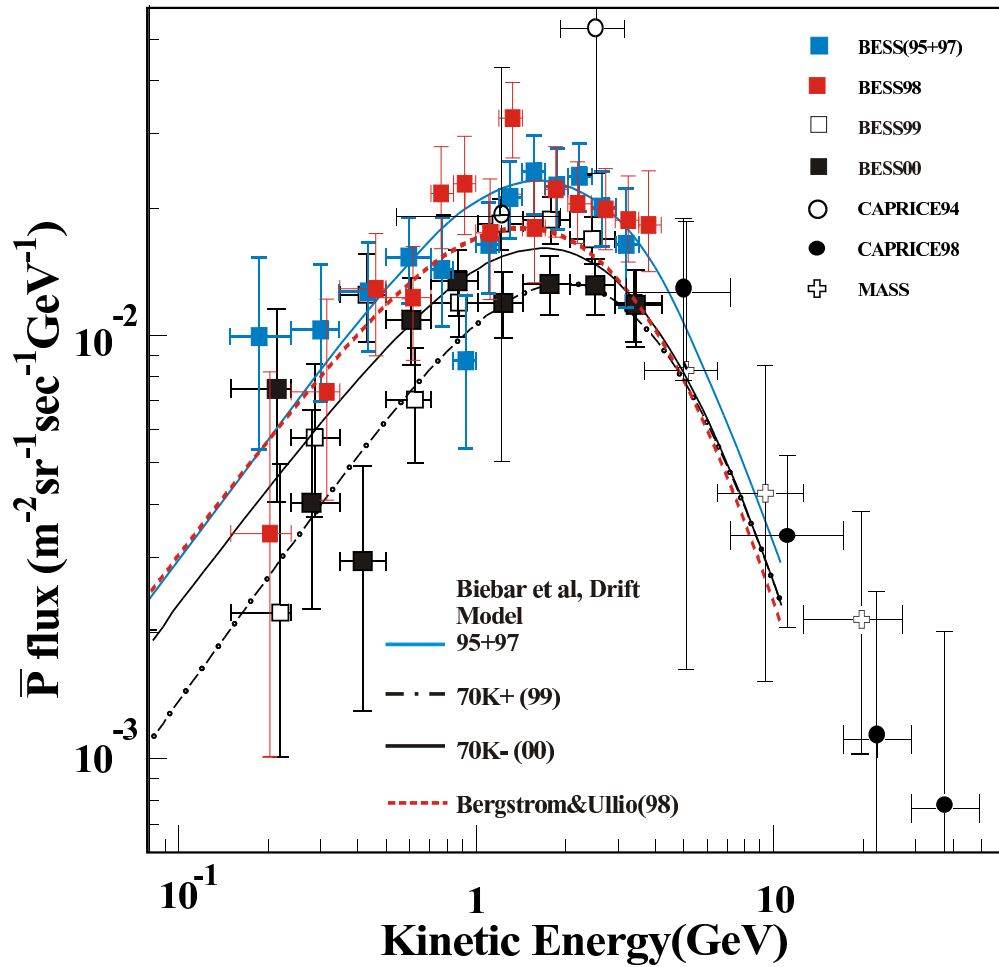


Figure 4.1: BESS 1995-2000 antiproton spectrum at the top of the atmosphere and CAPRICE and MASS data - The curves represent the theoretical calculations for secondary \bar{p} for the corresponding solar activity level [99].

4.1 Cosmic and Gamma rays indications for matter domination in the Universe

reported. They presented a precision measurement of the positron fraction in primary CR of 0.5-350 GeV and pointed to a new physical phenomena [104].

Thus, current CR results indicate that there is no antimatter objects within a radius 1 Mpc. However, the data are not definite for larger scales. In our work [99] we collected and studied the available data for \bar{p} observations and showed that they are consistent with the models of secondary production of antiparticles.

Gamma rays (GR) data, interpreted as a result from annihilation provides observational constraints on the antimatter fraction of different structures [105, 106, 107]. No evidence for annihilation features due to contacting matter and antimatter in the period $z < 100$ was found in the cosmic GR background. The measurements of the GR flux in the MeV region exclude significant amounts of antimatter up to the distance of galaxy cluster scales $\sim 10 - 20$ Mpc [105]. Hence, it is interesting to explore baryogenesis models predicting large antimatter structures.

The analysis of the relic GR contribution from early annihilation to the cosmic diffuse gamma spectrum gave the limit 1 Gpc in case of the following assumptions: matter-antimatter symmetric Universe, continuous close contact between domains of matter and antimatter and adiabatic perturbations [108]. This constraint is not applicable to isocurvature baryogenesis models [109], like the one discussed below, according to which there was not a close contact between matter and antimatter regions, and afterwards the separation increased. Besides, the assumption for the asymmetry is not obligatory! Antimatter regions may be less than the matter ones, then gamma observations constrain the antimatter-matter ratio at different scales.

The analysis of annihilation features within concrete baryogenesis model and the EGRET (Energetic Gamma Ray Experiment Telescope) [110] and Fermi Large Area Telescope [111] GR background data showed that even a small fraction ($< 10^{-6}$) of antimatter stars in our Galaxy is allowed! The allowed mass range $10^4 - 10^5 M_{Sun}$ corresponds to antistar globular cluster [112, 113]. And as we will discuss below, within the framework of the presented here baryogenesis model, antigalaxies and anticlusters may be a possibility, too. CR and GR data do not rule out antimatter domains in the Universe.

Other observational signatures of antimatter are *the distortion of the energy spectrum of the Cosmic Microwave Background Radiation and spatial variations of the*

primordial light elements abundances. The isotropy of CMB rules out large voids between matter and antimatter regions during earlier time. Successful BBN restricts the amount of annihilation at early pre-BBN epoch and, hence, puts stringent limits on the fraction of antimatter, in case it is in the $10^{-5} - 10$ pc i.e. sub-galaxy size range [114, 115].

4.2 Baryon density measurements

Since we know already that the Universe is baryon asymmetric in our vicinity, it is interesting to get the baryon asymmetry value, which at the present epoch is equal to the baryon density value η . Baryon density η is determined in several different ways: the most precise are from BBN, D measurements and from CMB.

The consistency between theoretically obtained and observationally measured abundances of the light elements produced in BBN at $z \sim 10^9$ [3] requires:

$$5.1 \times 10^{-10} \leq \eta_{BBN} \leq 6.5 \times 10^{-10} \quad \text{at} \quad 95\% \quad CL \quad (4.2)$$

The information for η from measurements of Deuterium towards low metallicity quasars combined with BBN data [4] points to:

$$\eta_D = 6 \pm 0.3 \times 10^{-10} \quad \text{at} \quad 95\% \quad CL \quad (4.3)$$

The most precise determination of η is provided by the measurements of the CMB anisotropy ($z \sim 1000$) by WMAP9 [5]:

$$\eta_{WMAP} = 6.16 \pm 0.16 \times 10^{-10} \quad \text{at} \quad 68\% \quad CL \quad (4.4)$$

The up-to-date data from Planck project [87] points to:

$$\eta_{Planck} = 6.05 \pm 0.09 \times 10^{-10} \quad \text{at} \quad 68\% \quad CL \quad (4.5)$$

These data presents the only known "experimental" indication for baryon violation.

In case this locally observed asymmetry is a *global* characteristic of the Universe, i.e. baryon asymmetry of the Universe (BAU), it may be due to the generation of a baryon excess at some early stage of the Universe, that diluted, eventually, during its further evolution gave the value observed today.

Due to considerations based on the existence of an inflationary period, it is known that BA may not be postulated as an initial condition and it should be generated in the Early Universe before BBN epoch [116].

Otherwise, in order to explain the BA generation, A. Sacharov postulated three necessary conditions: Baryon number violation (BV), C and CP violation and departure from thermal equilibrium [6].

In conclusion, we discussed the baryon density and antimatter asymmetry in our Universe. We reviewed the available data on antimatter detection in our vicinity. The explanation of the observed asymmetry, its sign and its value, is the main goal of the current baryogenesis scenarios. Today we do not yet know the exact baryogenesis mechanism, i.e. different baryogenesis possibilities are studied. Constraints from observational data are used to fix their parameters with the aim to find the realistic baryogenesis scenario.

4.3 Baryogenesis models

There are several interesting and possible mechanisms for the production of the baryon asymmetry. The three most popular among them are:

GUT (Great Unified Theories) Baryogenesis model - This was historically the first model [6, 117] and it was based on the out of equilibrium decay of a massive particle such as a superheavy GUT gauge or Higgs boson. Due to C and CP violation the partial widths of decays into channels with different baryonic numbers should be different. Such a mechanism can be realized with a gauge boson with $m_X = 10^{16}$ GeV. The baryogenesis is most efficient at $T \sim m_X$. The problem of this model is that the Universe has never reached such a temperature after inflation and CP violation is insufficient to explain the observed today value.

Electroweak baryogenesis [7] - There is also the possibility of generating the baryon asymmetry at the electro-weak scale using the non-perturbative interactions of sphalerons [118]. Generation of baryon asymmetry in this scenario takes place not in massive particle decays but on the boundary between two phases with unbroken and broken $SU(2) \times U(1)$ symmetry of weak interactions respectively. In the high energy phase the symmetry is unbroken and B is not conserved. In the low temperature phase B is practically conserved but if the phase transition was first order on the boundary

between two phases B non-conservation and deviation from thermal equilibrium could be strong enough to generate the observed baryon asymmetry. However, heavy Higgs boson, $m_X > 100$ GeV leads to the second order phase transition and to very weak deviation from thermal equilibrium.

Baryo-through-lepto-genesis [8] is a combination of the first two models. In this scenario lepton asymmetry was generated at temperatures about 10^{10} GeV in the decays of a heavy Majorana fermion and after that it was distributed between baryon and lepton asymmetries in almost equal share by the equilibrium electroweak processes which conserve (B - L) but break (B + L).

An interesting mechanism involving the decay of flat directions in supersymmetric models is known as the *Affleck-Dine scenario* [9]. In supersymmetric models there must exist scalar superpartner of baryons and leptons φ . The potential $U(\varphi)$ of such scalar field has flat directions along which the field can have a non-zero vacuum expectation values due to quantum fluctuations during inflation. After inflation φ evolves down to the mechanical equilibrium point $\varphi = 0$ and if the potential $U(\varphi)$ is not symmetric with respect to the phase rotation it acquires non-vanishing and typically large baryonic charge. Subsequent B-conserving decay of φ into quarks and leptons transform baryon (or lepton) asymmetry into the quarks sector. In contrast to other scenarios of baryogenesis, this one normally leads to higher value of β and additional mechanisms are needed to dilute it down to the observed value.

In series of papers Scalar field condensate (SFC) baryogenesis model [1, 99, 109, 119, 120, 121, 122, 123], based on the Affleck and Dine baryogenesis scenario was explored. The complex scalar field φ is a scalar superpartner of a colorless and electrically neutral combination of quark and lepton fields. The condensate $\langle \varphi \rangle \neq 0$ is formed during the inflationary period if baryon charge B and lepton charge L were not conserved as a result of the rise of quantum fluctuations of the φ field [124, 125, 126, 127]: $\langle \varphi^2 \rangle = H^3 t / 4\pi^2$ until the limiting value $\langle \varphi^2 \rangle \sim H^2 / \sqrt{\lambda}$ in case that $\lambda\varphi^4$ dominates in the potential energy of φ .

The baryon charge of the field is not conserved at large field amplitude due to the presence of the B nonconserving self-interaction terms in its potential. Due to that, during inflation a condensate of a baryon charge (stored in $\langle \varphi \rangle$) is developed with a baryon charge density $\sim H_I^3$, where H_I is the Hubble parameter at the inflationary stage.

4.3 Baryogenesis models

In case Γ is a decreasing function of time the damping process may be slow enough for the baryon charge contained in φ to survive until the B-conservation epoch [109].

At low φ baryon violation (BV) becomes negligible. At the B conserving stage the baryon charge contained in the field is transferred to that of quarks during the decay of the field $\varphi \rightarrow q\bar{q}l\gamma$. As a result a baryon asymmetric plasma appears. This asymmetry, eventually further diluted during the following evolution of the Universe, gives the present baryon asymmetry of the Universe.

The model has two more interesting features: unharmonic potential of the field carrying the baryon charge, which provides that different amplitudes corresponding to different space points result into different periods and hence, the initially smooth space dependence transfers into quasiperiodic one and inflationary expansion of the initially microscopic baryon distribution (see for example [120, 128]). This baryogenesis model is capable to provide a natural separation mechanism of considerable quantities of matter from antimatter ones. There exist different inhomogeneous baryogenesis models, which predict matter and antimatter regions [129]. Our model is one of them and it predicts vast regions of antimatter, safely separated from the matter ones, so that the CR and GR constraints are satisfied [99].

We discussed briefly the most popular baryogenesis models and more precisely a SCF baryogenesis model, based on the Affleck-Dine scenario. We chose to use this model to examine the possibility of producing the observed baryon asymmetry.

5

Scalar field condensate baryogenesis scenario

We examine the case when after inflation there exist two scalar fields - the inflaton ψ and the scalar field φ and the inflaton density dominates: $\rho_\psi > \rho_\varphi$. Hence, when at the end of the inflation period $\psi = m_{PL}(3\pi)^{-1/2} \sin(m_\psi t)$ the Hubble parameter is $H = 2/(3t)$.

In the expanding Universe, φ satisfies the equation of motion:

$$\ddot{\varphi} - a^{-2}\partial_i^2\varphi + 3H\dot{\varphi} + \frac{1}{4}\Gamma\dot{\varphi} + U'_\varphi = 0, \quad (5.1)$$

where $a(t)$ is the scale factor and $H = \dot{a}/a$, Γ accounts for the particle creation processes and $U(\varphi)$ is the field potential. In our model, we choose the form of the potential as follows:

$$U(\varphi) = m^2\varphi^2 + \frac{\lambda_1}{2}|\varphi|^4 + \frac{\lambda_2}{4}(\varphi^4 + \varphi^{*4}) + \frac{\lambda_3}{4}|\varphi|^2(\varphi^2 + \varphi^{*2}) \quad (5.2)$$

The mass parameters of the potential are assumed small in comparison with the Hubble constant during inflation $m \ll H_I$. In supersymmetric theories the self coupling constants λ_i are of the order of the gauge coupling constant α . A natural range of m is $10^2 - 10^4$ GeV.

The initial values for the field variables can be derived from the natural assumption that the energy density of φ at the inflationary stage is of the order H_I^4 , then

$$\varphi_o^{max} \sim H_I\lambda^{-1/4} \text{ and } \dot{\varphi}_o = (H_I)^2. \quad (5.3)$$

5.1 Description and assumptions of the model

After inflation φ starts to oscillate around its equilibrium point and its amplitude decreases due to the Universe expansion and the particle creation by the oscillating scalar field.

5.1 Description and assumptions of the model

To proceed with our numerical analysis, first we had to solve the system of ordinary differential equations, corresponding to the equation of motion for the real and imaginary part of $\varphi = x + iy$:

$$\begin{aligned}\ddot{x} + 3H\dot{x} + \frac{1}{4}\Gamma_x\dot{x} + (\lambda + \lambda_3)x^3 + \lambda'xy^2 &= 0 \\ \ddot{y} + 3H\dot{y} + \frac{1}{4}\Gamma_y\dot{y} + (\lambda - \lambda_3)y^3 + \lambda'yx^2 &= 0\end{aligned}\quad (5.4)$$

where $\lambda = \lambda_1 + \lambda_2$, $\lambda' = \lambda_1 - 3\lambda_2$.

It is convenient to make the substitutions $x = H_I(t_i/t)^{2/3}u(\eta)$, $y = H_I(t_i/t)^{2/3}v(\eta)$ where $\eta = 2(t/t_i)^{1/3}$. Then the functions $u(\eta)$ and $v(\eta)$ satisfy the equations:

$$\begin{aligned}u'' + 0.75 \alpha\Omega_u(u' - 2u\eta^{-1}) + u[(\lambda + \lambda_3)u^2 + \lambda'v^2 - 2\eta^{-2} + \frac{m^2}{H}\eta^4] &= 0 \\ v'' + 0.75 \alpha\Omega_v(v' - 2v\eta^{-1}) + v[(\lambda - \lambda_3)v^2 + \lambda'u^2 - 2\eta^{-2} + \frac{m^2}{H}\eta^4] &= 0.\end{aligned}\quad (5.5)$$

The initial conditions in the new variables are:

$$\begin{aligned}u_0(\eta) = \lambda^{-0.25}2^{0.25} \cos p, \quad v_0(\eta) = \lambda^{-0.25}2^{0.25} \sin p \quad \text{and} \\ u'_0 = 3/2^{1.5} + \lambda^{-0.25}2^{0.25} \cos p, \quad v'_0 = 3/2^{1.5} + \lambda^{-0.25}2^{0.25} \sin p.\end{aligned}\quad (5.6)$$

where p is the angle.

The baryon charge in the comoving volume $V = V_i(t/t_i)^2$ is

$$B = N_B \cdot V = 2(u'v - v'u).\quad (5.7)$$

5.2 Numerical study of the scalar field and baryon number evolution

We have developed a computer program in fortran 77 to solve the system of ordinary differential equations 5.5, corresponding to the equation of motion for the real and imaginary part of φ and B contained in it, using Runge-Kutta 4th order method. The program is presented in Appendix 1. The Runge-Kutta 4th order routine is used from [130]. In the program Ω_u and Ω_v are calculated at each step in separate routine procedures. Because of the complexity of the task it needs serious computational resources. A single calculation depending as the concrete parameters set takes between several hours and three weeks. The analysis contains dozens of parameters sets calculations.

We studied numerically the evolution of $\varphi(t)$ and B(t) in the period after inflation until the BC epoch. The typical range of energies discussed is $10^{12} - 100$ GeV. We analyzed φ and B evolution for natural ranges of values of the model's parameters: $\lambda = 10^{-2} - 5 \times 10^{-2}$, $\alpha = 10^{-3} - 5 \times 10^{-2}$, $H = 10^7 - 10^{12}$ GeV, $m = 100 - 1000$ GeV.

In summary, we based our precise numerical analysis on solving the system of ordinary differential equations, corresponding to the equation of motion for the real and imaginary part of the scalar field. We described the steps providing our calculations and analysis.

6

Results from the numerical analysis of the model

6.1 Role of particle creation processes

Particle creation processes play essential role for the determination of β [109, 119], hence it is important to account for them as precisely as possible.

Fast oscillations of φ result in particle creation due to the coupling of the scalar field to fermions $g\varphi\bar{f}_1f_2$, where $g^2/4\pi = \alpha$ [119, 120]. The term $\Gamma\dot{\varphi}$ in the equations of motion 5.4 accounts for the damping of φ as a result of particle production processes, namely the amplitude of φ is damped as $\varphi \rightarrow \varphi \exp(-\Gamma t/4)$. Hence, in case $\Gamma = \text{const}$ the baryon charge, contained in the φ condensate, is reduced exponentially due to particle creation at this stage with considerable baryon violation and will not survive till φ decays to quarks and leptons and transfers its charge to the matter components of today's Universe.

In ref. [1] we accounted for particle production processes in two different ways, namely qualitatively - using the analytical form for $\Gamma = \alpha\Omega$, where the frequency Ω is estimated as $\Omega \sim \lambda^{1/2}\varphi$, $g^2/4\pi = \alpha$, and quantitatively - calculating numerically Ω at each step.

We solved the system of ordinary differential equations, corresponding to the equation of motion for the real and imaginary part of φ , by Runge-Kutta 4th order method for both cases. We have found that the results for φ and B evolution and the final value of B at BC epoch considerably differ when different accounts for particle creation processes

6.2 Dependence on the model parameters

are made [1, 122].

In Fig. 6.1 and Fig. 6.2 we illustrate the evolution $B(\eta)$ for fixed model's parameters $\lambda_1 = 5 \times 10^{-2}$, $\lambda_2 = \lambda_3 = 5 \times 10^{-4}$, $\alpha = 10^{-3}$, $H = 10^{11} \text{ GeV}$, $m = 350 \text{ GeV}$, $\varphi_o = 2^{-1/4} H \lambda^{-1/4}$, and $\dot{\varphi}_o = H^2$, and in two different cases, namely when the particle creation is accounted either numerically or analytically [1].

The amplitude of B_{num} decreases more sharply than the amplitude of B_{anal} and hence at BC epoch $B_{num} = -2.2 \times 10^{-3}$ and $B_{anal} = -1.7 \times 10^{-2}$. The difference is considerable. *Therefore, a precise numerical description for the account of particle creation processes is necessary when constructing a realistic baryogenesis model.*

Further the analysis is provided for another set of parameters, namely $\lambda_1 = 5 \times 10^{-2}$, $\lambda_2 = \lambda_3 = 10^{-3}$, $\alpha = 10^{-2}$, $H = 10^{10} \text{ GeV}$, $m = 350 \text{ GeV}$ [123]. As it was found in previous publications [1, 109], the account of particle creation processes strongly reduces the amplitude of the baryon asymmetry contained in the condensate. The more exact numerical account of the particle creation effect in this analysis points to stronger and earlier reduction of the generated baryon excess (see Fig. 6.3). The values of final B, obtained with numerical and analytical account of particle creation, may differ by up to two orders of magnitude.

It has been found that due to the oscillatory character of B, the generated BA is very sensitive both to small shifts of the model's parameters and to numerical methods used. Nevertheless, it is possible to determine the main trend of the dependence of the final BA on the parameters values.

Here we followed the scalar field and baryon charge evolution through time with analytical and numerical calculation of particle production rate. We showed that a precise numerical account for Γ is necessary to provide accurate analysis since the difference in the obtained results is up to two orders of magnitude in comparison with the analytical case.

6.2 Dependence on the model parameters

We have calculated β produced for different range of model's parameters - gauge coupling constant α , Hubble constant during inflation H_i , mass of the condensate m and self coupling constants λ_i .

6.2 Dependence on the model parameters

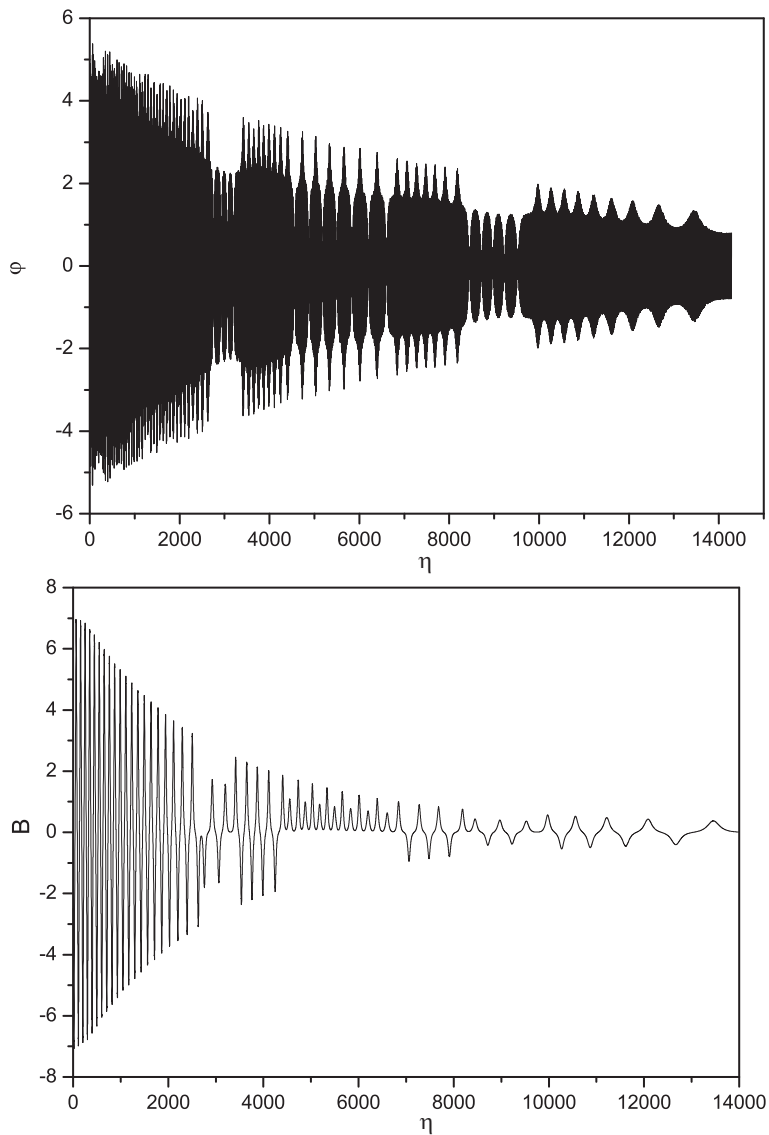


Figure 6.1: Field and B evolution with analytically accounted particle creation processes. - The evolution of the scalar field $\varphi(\eta)$ and the baryon charge $B(\eta)$ for $\lambda_1 = 5 \times 10^{-2}$, $\lambda_2 = \lambda_3 = 5 \times 10^{-4}$, $\alpha = 10^{-3}$, $H = 10^{11}$ GeV, $m=350$ GeV, $\varphi_o = 2^{-1/4}H\lambda^{-1/4}$ and $\dot{\varphi}_o = H^2$ [1].

6.2 Dependence on the model parameters

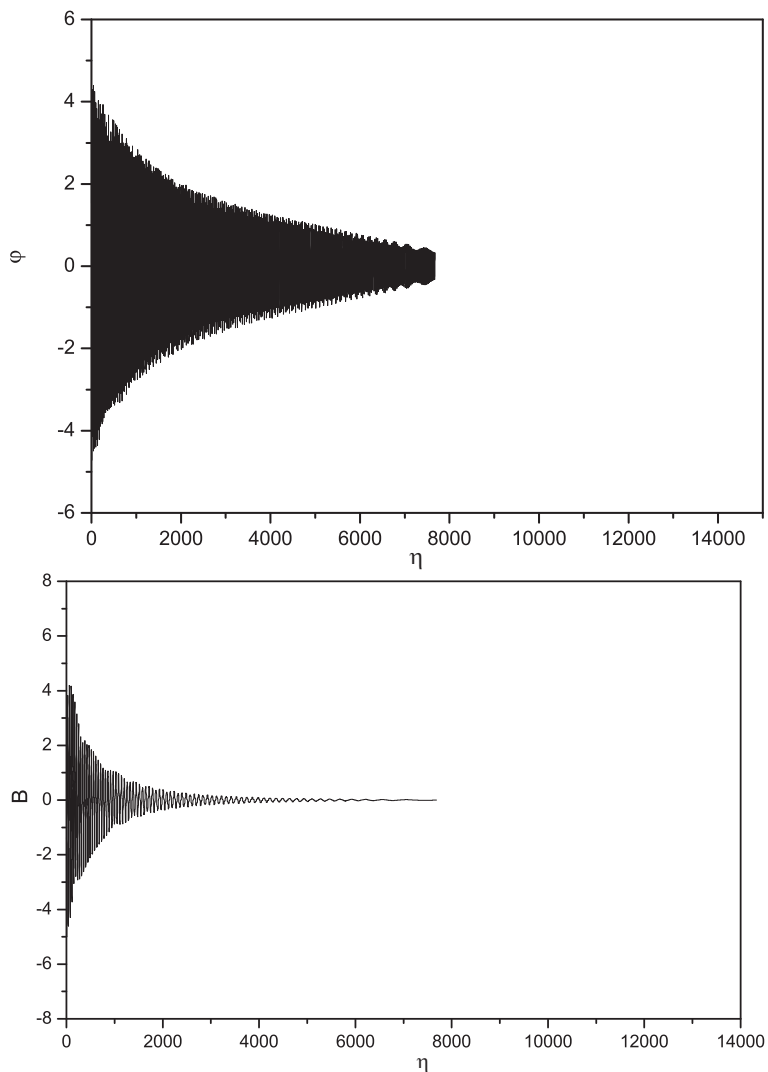


Figure 6.2: Field and B evolution with numerically accounted particle creation processes. - The evolution of the scalar field $\varphi(\eta)$ and baryon charge $B(\eta)$ for $\lambda_1 = 5 \times 10^{-2}$, $\lambda_2 = \lambda_3 = 5 \times 10^{-4}$, $\alpha = 10^{-3}$, $H = 10^{11}$ GeV, $m=350$ GeV, $\varphi_o = 2^{-1/4}H\lambda^{-1/4}$, and $\dot{\varphi}_o = H^2$ [1].

6.2 Dependence on the model parameters

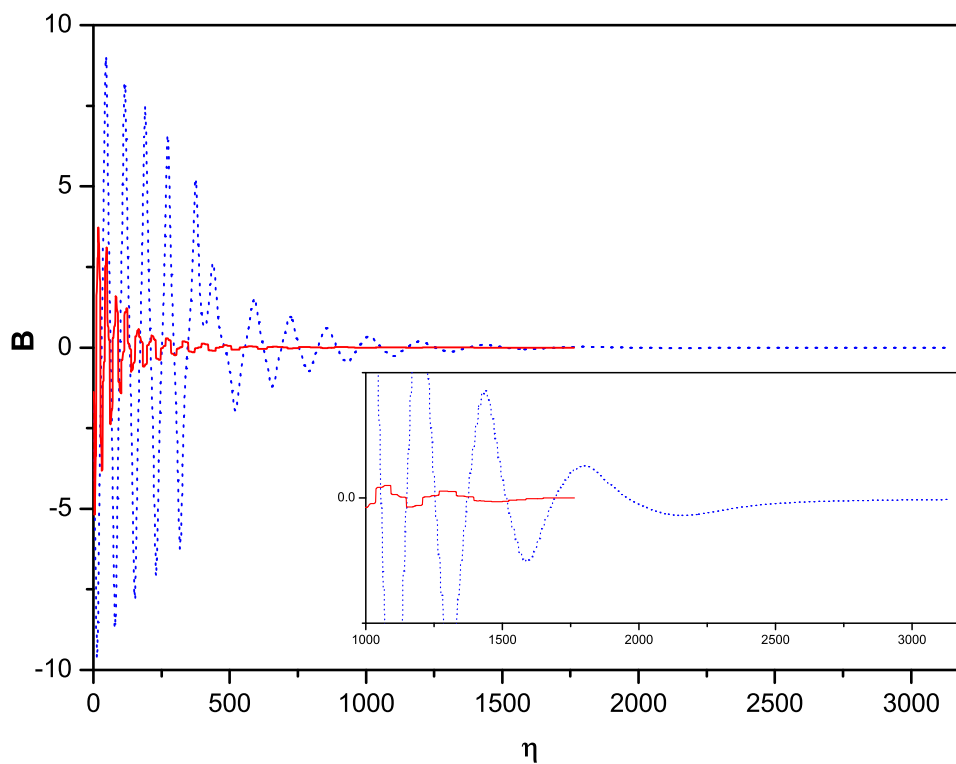


Figure 6.3: The evolution of the baryon charge $B(\eta)$ for $\lambda_1 = 5 \times 10^{-2}$, $\lambda_2 = \lambda_3 = 10^{-3}$, $\alpha = 10^{-2}$, $H = 10^{10}$ GeV, $m=350$ GeV, $\varphi_o = H_I \lambda^{-1/4}$ and $\dot{\varphi}_o = H_I^2$. - The case of particle creation processes accounted for analytically is presented by the dotted curve and the case of numerical account for the particle creation is given by the solid curve [123].

6.2 Dependence on the model parameters

6.2.1 Dependence on gauge coupling constant α

Using the numerical account for Γ we have calculated $B(t)$ for α varying in the range $10^{-3} - 10^{-2}$ and fixed other parameters [1, 122]. The dependence of B on α is very strong, as can be expected, knowing that particle creation processes play essential role for the evolution of the field and the baryon charge, contained in it, and keeping in mind that the analytical estimation is $\Gamma = \alpha\Omega$.

With increasing α , B evolution becomes shorter and the final B decreases. An illustration of this dependence $B(\alpha)$ is given in Fig. 6.4.

6.2.2 Dependence on Hubble constant during inflation H_I

We have followed the evolution $B(t)$ varying H_I for fixed values of the other parameters [1]. Our analysis shows that *B evolution becomes longer and the final B value decreases with H_I increase.* The results are presented in Fig. 6.5.

The next figure (Fig. 6.6) presents the dependence of the generated baryon charge on the value of H_I for different set of fixed parameters. The numerical study again shows that the produced baryon charge decreases when increasing H_I . Qualitatively, this dependence is an expected result because the initial value of φ is proportional to H_I and on the other hand particle creation is proportional to φ , $\Gamma \sim \Omega \sim \varphi$.

6.2.3 Dependence on the mass m of the condensate

We have calculated $B(t)$ when varying m for fixed $\lambda_1, \lambda_2, \lambda_3, \alpha$ and H_I [1]. The analysis of our results shows that *for lower values of m , B evolution is longer and the final B value is greater.* This behavior of η corresponds to the expected one, as far as m defines the onset of BC epoch: $t_{stop} \sim 1/\alpha m$. The dependence is illustrated in Fig. 6.7.

The following figure (Fig. 6.8) presents the dependence of the baryon charge, at the BC epoch, on the mass of the condensate for another set of parameters of the model. It seems that the dependence on m does not correspond to the expected one, hence it is more complicated to be estimated analytically.

6.2.4 Dependence on self coupling constants λ_i

Further we have provided numerical study of the evolution of B and φ to explore also the dependence of the B generation on the self coupling constants λ_i [123]. As

6.2 Dependence on the model parameters

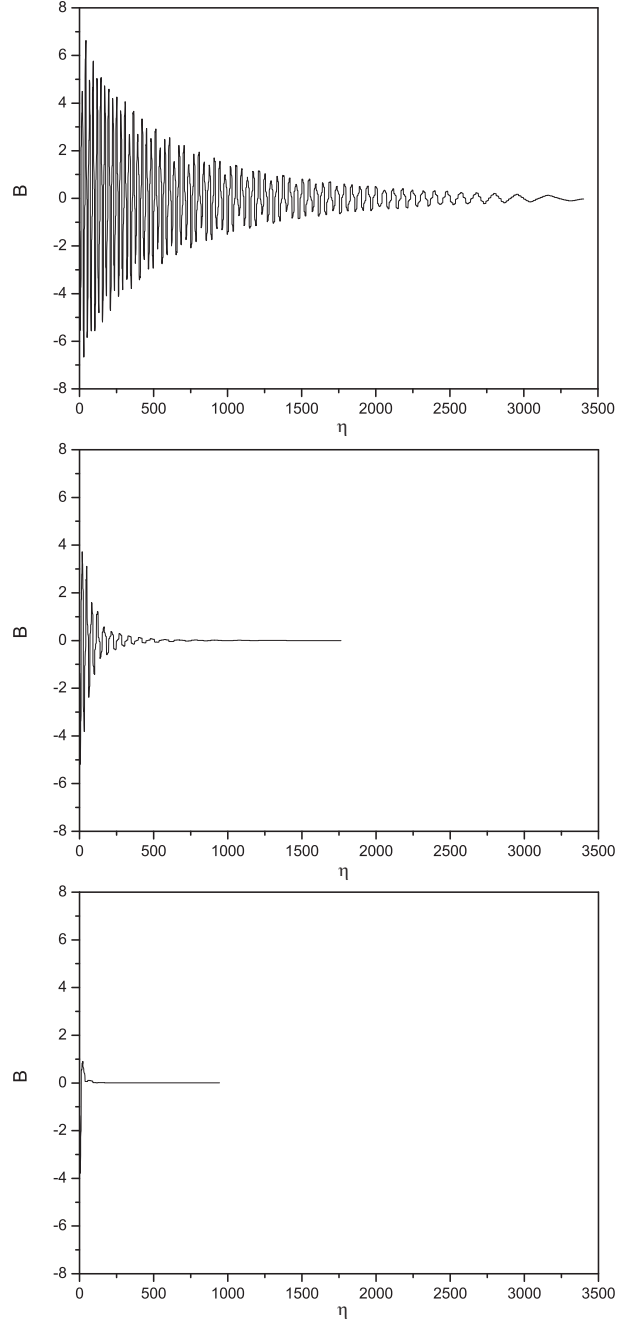


Figure 6.4: The evolution of the baryon charge $B(\eta)$ for $\lambda_1 = 5 \times 10^{-2}$, $\lambda_2 = \lambda_3 = 10^{-3}$, $H = 10^{10}$ GeV, $m = 350$ GeV, $\varphi_o = H_I \lambda^{-1/4}$ and $\dot{\varphi}_o = H_I^2$. - The upper curve is for $\alpha = 10^{-3}$, the middle curve is for $\alpha = 10^{-2}$, the lower curve is for $\alpha = 5 \times 10^{-2}$. The particle creation processes are accounted for numerically [1].

6.2 Dependence on the model parameters

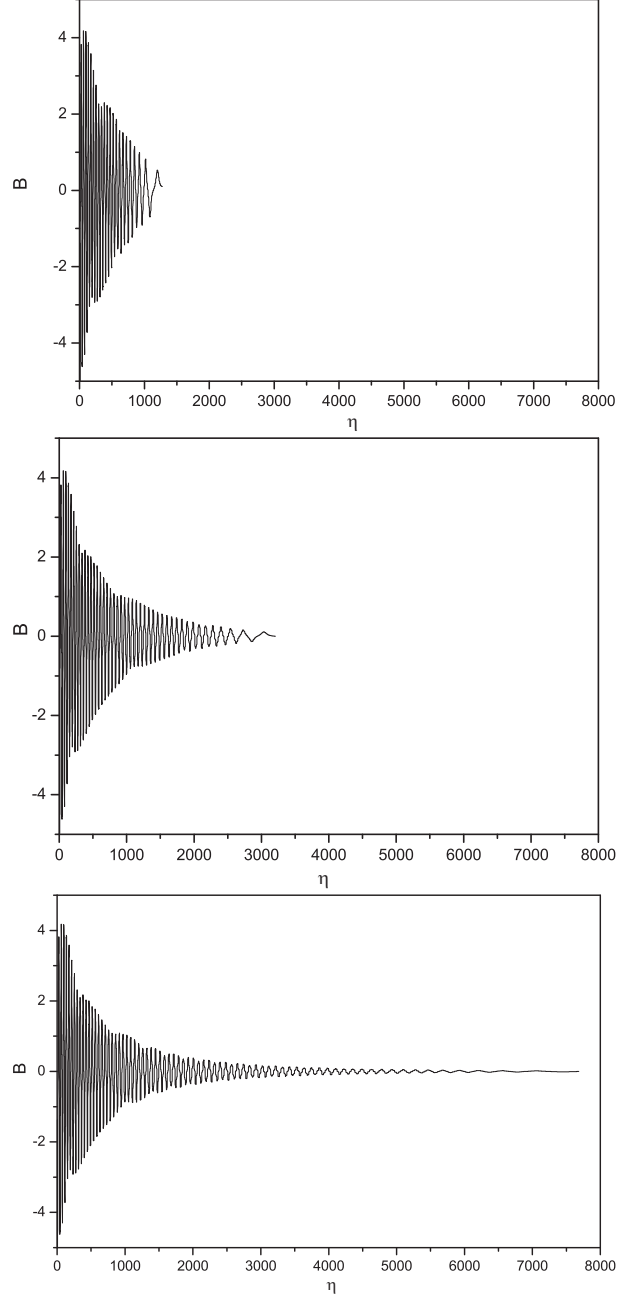


Figure 6.5: The evolution of the baryon charge $B(\eta)$ for $\lambda_1 = 5 \times 10^{-2}$, $\lambda_2 = \lambda_3 = 5 \times 10^{-4}$, $\alpha = 10^{-3}$, $m = 350$ GeV, $\varphi_o = H_I \lambda^{-1/4}$ and $\dot{\varphi}_o = H_I^2$. - The upper curve is for $H = 10^9$ GeV, the middle curve is for $H = 10^{10}$ GeV, the lower curve is for $H = 10^{11}$ GeV. The particle creation processes are accounted for numerically [1].

6.2 Dependence on the model parameters

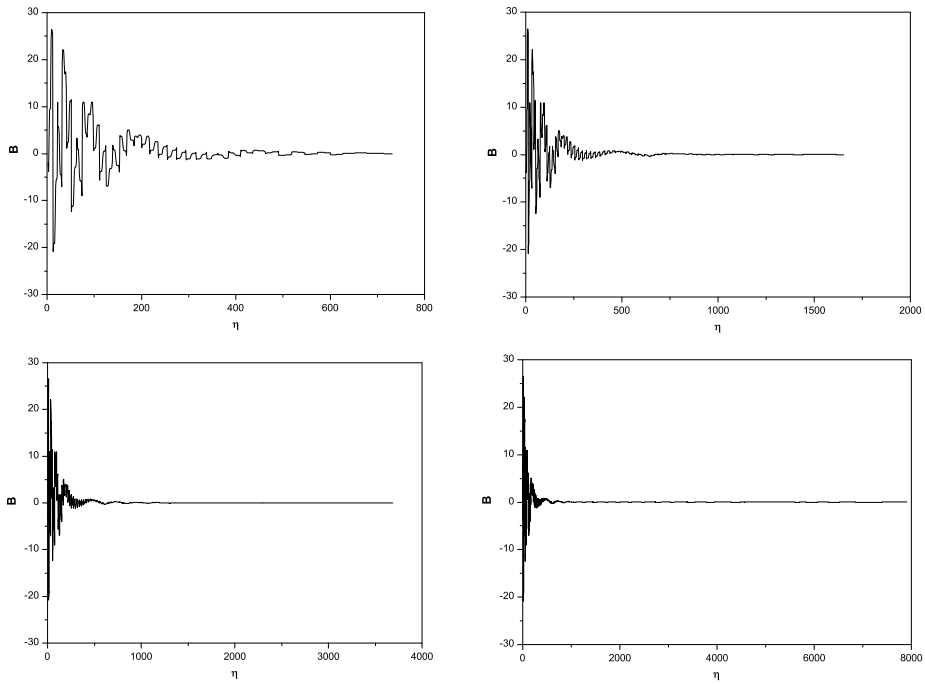


Figure 6.6: The evolution of the baryon charge $B(\eta)$ for $\lambda_1 = 10^{-2}$, $\lambda_2 = \lambda_3 = 10^{-3}$, $\alpha = 10^{-2}$, $m=500$ GeV, $\varphi_o = H_I \lambda^{-1/4}$ and $\dot{\varphi}_o = H_I^2$. - The upper left curve is for $H = 10^9$ GeV, the upper right curve is for $H = 10^{10}$ GeV, the lower left curve is for $H = 10^{11}$ GeV and the lower right curve - for $H = 10^{12}$ GeV. The particle creation processes are accounted for numerically [123].

6.2 Dependence on the model parameters

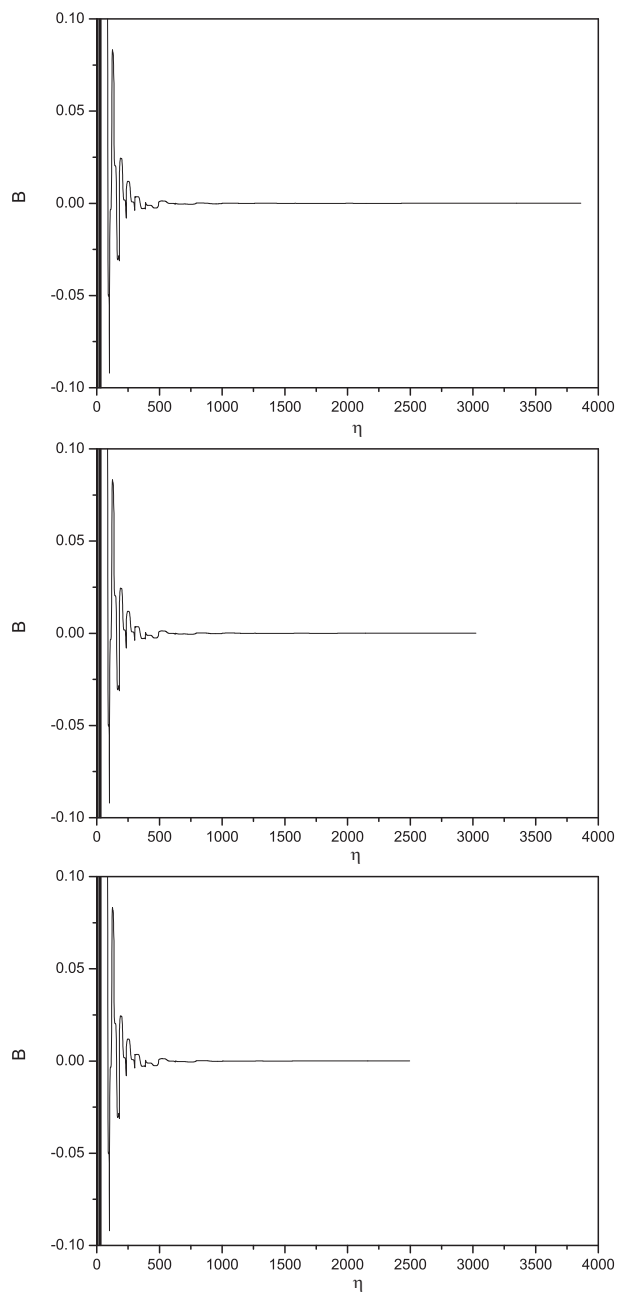


Figure 6.7: The evolution of the baryon charge $B(\eta)$ for $\lambda_1 = 5 \times 10^{-2}$, $\lambda_2 = \lambda_3 = 10^{-2}$, $\alpha = 5 \times 10^{-2}$, $H = 10^{11}$ GeV, $\varphi_o = H_I \lambda^{-1/4}$ and $\dot{\varphi}_o = H_I^2$. - The upper curve is for $m = 100$ GeV, the middle curve is for $m = 200$ GeV, the lower curve is for $m = 350$ GeV. The particle creation processes are accounted for numerically [1].

6.2 Dependence on the model parameters

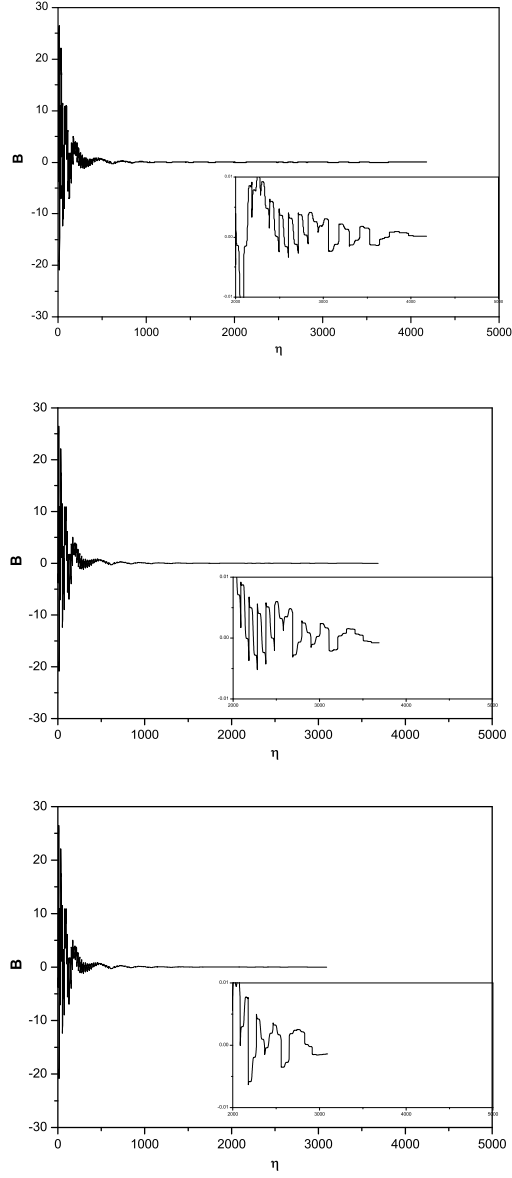


Figure 6.8: The evolution of the baryon charge $B(\eta)$ for $\lambda_1 = 10^{-2}$, $\lambda_2 = \lambda_3 = 10^{-3}$, $\alpha = 10^{-2}$, $H = 10^{11}$ GeV, $\varphi_o = H_I \lambda^{-1/4}$ and $\dot{\varphi}_o = H_I^2$. - The upper curve is for $m=350$ GeV, the middle is for $m=500$ GeV and the lower - for $m=800$ GeV. The particle creation processes are accounted for numerically [123].

6.3 Inhomogenous scalar field condensate baryogenesis model

far as λ_i constants are not known, it is interesting to find the allowed range of these parameters corresponding to the successful B generation. The following values of the model parameters are analyzed: $\alpha = 10^{-3}$, $H = 10^{12}$ GeV, $m = 350$ GeV while varying λ_i in the ranges: $\lambda_1 = 10^{-3} - 3 \times 10^{-2}$ and $\lambda_{2,3} = 5 \times 10^{-4} - 5 \times 10^{-3}$.

It has been shown that the effect of λ_i variation within the studied range is enough to produce a difference in the final B value of an order of magnitude.

Fig. 6.9 presents the dependence of the baryon charge, at the BC epoch, on λ_1 constant. The analysis shows that *with increasing of λ_1 B evolution becomes shorter*. In this parameters range, it is not possible to make a definite conclusion on how the final B value depends on λ_1 .

In Fig. 6.10 results for the dependence of B and the final B value on $\lambda_{2,3}$ are presented. In this case the *evolution of B tends to become longer with increasing $\lambda_{2,3}$ and the final value of B decreases*. The effect is not very significant but still provides a difference in the final B value of an order of magnitude.

6.3 Inhomogenous scalar field condensate baryogenesis model

One of the interesting features of our model is that it may predict vast regions of antimatter, safely separated from the matter ones [99, 123]. The necessary conditions for generation of vast separated regions of matter and antimatter in this scenario are: initial space distribution $\varphi(r, t_0)$, unharmonic potential and inflationary expansion.

We studied the evolution of the baryonic space distribution, assuming a monotonic initial distribution of the baryon density within a domain with a certain sign of the baryon number $\varphi(r, t_0)$. For different sets of parameter values of the model $\lambda_i, \alpha, m/H_I$, we have numerically followed the evolution $B(t, r)$ for all initial values of the field $\varphi_0^i = \varphi(r_i, t_0)$ till t_B . In case of nonharmonic fields potential, the initially monotonic space behavior is quickly replaced by space oscillations of φ , because of the dependence of the period on the amplitude [128].

In our model the dependence is $\omega \sim \lambda^{1/2} \varphi_i(r)$. As a result in different points different periods are observed and spatial behavior of φ becomes quasiperiodic. Correspondingly, the spatial distribution of baryons $B(t_B, r)$ at the moment of baryogenesis is found to be quasiperiodic. The region r_0 which initially was characterized with its

6.3 Inhomogeneous scalar field condensate baryogenesis model

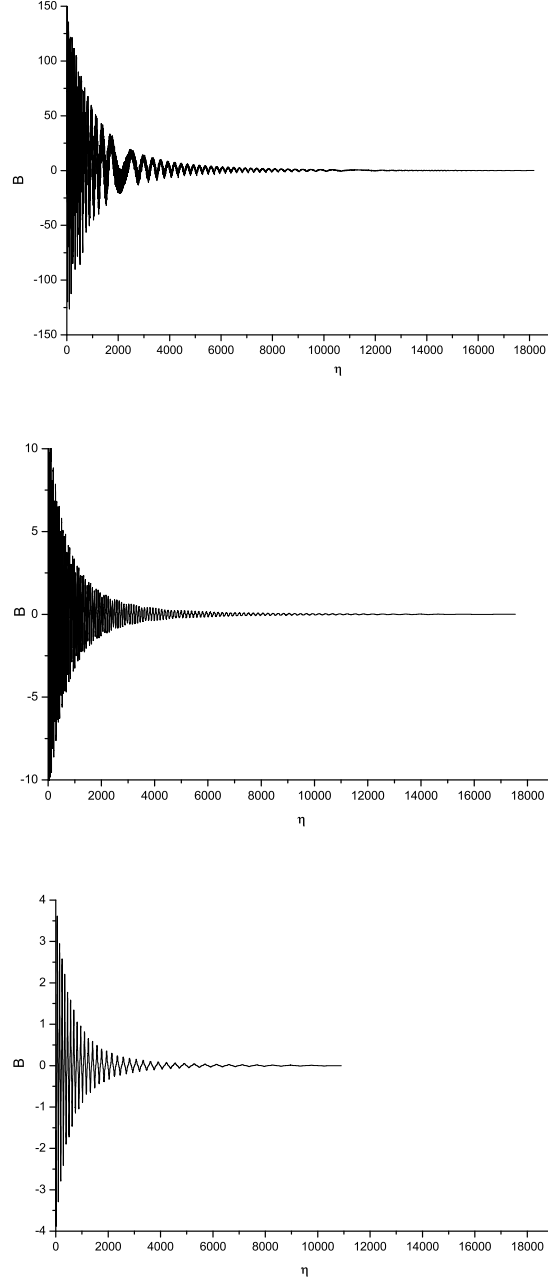


Figure 6.9: The evolution of the baryon charge $B(\eta)$ for $\alpha = 10^{-3}$, $m=350$ GeV, $H = 10^{12}$ GeV, $\lambda_{2,3} = 10^{-4}$, $\varphi_o = H_I \lambda^{-1/4}$ and $\dot{\varphi}_o = H_I^2$. - The upper curve is for $\lambda_1 = 10^{-3}$, the middle is for $\lambda_1 = 10^{-2}$ and the lower - for $\lambda_1 = 3 \times 10^{-2}$. The particle creation processes are accounted for numerically [2].

6.3 Inhomogeneous scalar field condensate baryogenesis model

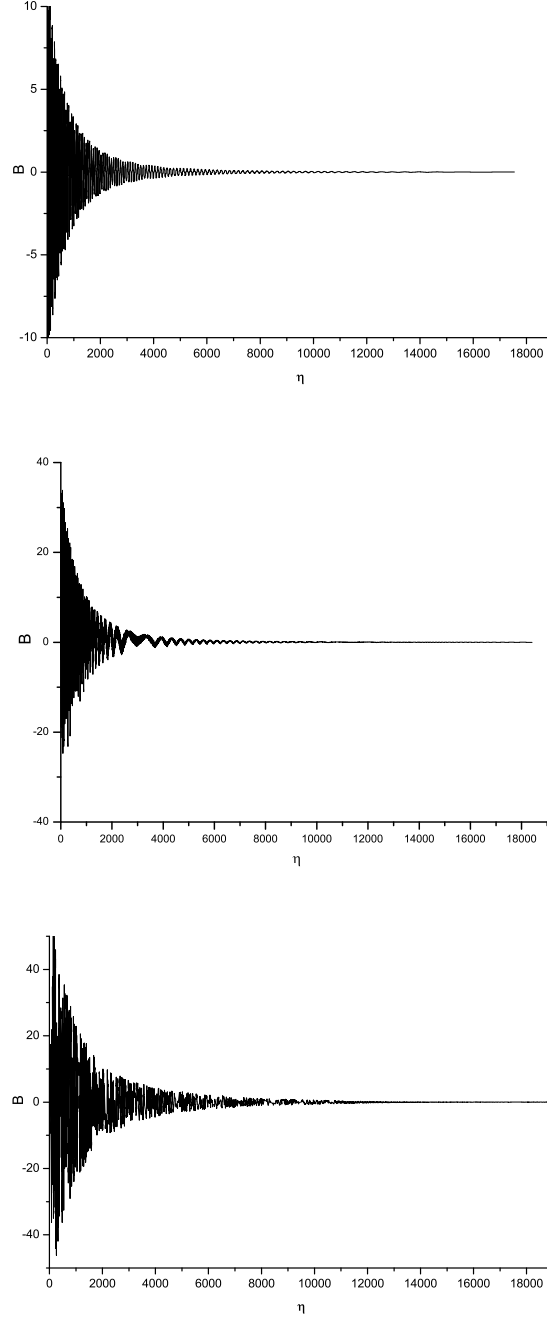


Figure 6.10: The evolution of the baryon charge $B(\eta)$ for $\alpha = 10^{-3}$, $m=350$ GeV, $H = 10^{12}$ GeV, $\lambda_1 = 10^{-2}$, $\varphi_o = H_I \lambda^{-1/4}$ and $\dot{\varphi}_o = H_I^2$. - The upper curve is for $\lambda_{2,3} = 10^{-4}$, the middle is for $\lambda_{2,3} = 10^{-3}$ and the lower - for $\lambda_{2,3} = 5 \times 10^{-3}$. The particle creation processes are accounted for numerically [2].

6.3 Inhomogeneous scalar field condensate baryogenesis model

baryon excess splits into regions with baryon excess and such of baryon underdensities [120]. Due to the smoothly decreasing baryon density towards the borders between the baryonic and antibaryonic regions, predicted by the model, annihilation is not considerable at t_B . After that, the baryon and antibaryon regions further contract towards their centers, where density is higher. Hence, matter and antimatter domains become separated by large empty from baryons voids, perhaps filled with dark matter. Thus the stringent limit [108] on antimatter domains is evaded.

Two cases are possible. In the first one, Stochastic CP-violation, the variations appear around zero baryon charge. The initially baryonic domain is broken to baryonic and antibaryonic regions and divided by nearly baryonically empty space. The case is attractive as far as it allows the realization of a symmetric Universe without domain walls. However, the resulting fluctuations of the baryon density may be considerable and lead to unacceptably large angular variations of the microwave background radiation.

In the second case, stochastic+explicit CP-violation, the field's equilibrium value is non zero, and the fluctuations of the field around it result into fluctuations of the baryon density around some mean number. Then at t_B the domain with a given sign of explicit CPV may consist predominantly of baryonic regions plus small quantity (for $l \sim 100$ Mpc it is $\sim 10^{-4}$) of antibaryonic ones. Though not so aesthetic, because in that case there should be besides the stochastic CPV discussed, another mechanism of CPV producing the mean baryon density, this case is more promising.

Due to inflation the regions with different baryon density (overdensity, underdensity or density of antibaryons) become macroscopically large $d \rightarrow d \exp(Ht)$. The characteristic scale between matter and antimatter regions is a function of the models parameters, namely the coupling constants of the potential λ_i , the initial amplitudes of the field $\phi(r, t_i)$, the period of baryogenesis t_b and the characteristic scale of the baryon space variation at the inflationary stage r_o . The provided analysis showed that for a natural choice of the values of these parameters the separation scale may be in the Mpc - 100 Mpc range.

Using the constraints from GR and CR data, BBN and CMB anisotropy measurements, it is interesting to discuss different realizations of the model. Recent CMB measurements ruled out pure isocurvature perturbations models, so, accordingly, the case when the baryon charge carrying field is the inflaton itself, is excluded. Other

6.3 Inhomogeneous scalar field condensate baryogenesis model

possibilities, when besides the inflaton there exists a second scalar field during inflation with the features discussed in our model remain viable [131]. According to the recent mixed isocurvature plus adiabatic models, although the isocurvature contribution is not suggested it has neither been ruled out.

In the case of stochastic CP-violation, two possibilities are discussed. The first most simple case considered in [121] aiming to explain the observed 120 Mpc periodicity in the visible matter distribution, assumed that the overdensity regions correspond to galaxy or antigalaxy superclusters with big voids between with a characteristic size ~ 120 Mpc. In that case the antimatter domains are roughly of the same scale and the similar density as the matter ones. CR and GR data constraints are fulfilled. Large variation of the primordially produced elements, should be observable at the corresponding scales. There are no data for the rest light elements at large distances, however the observed D towards high- z quasars shows some deviations from the expected primordial plateau. Alas, in that case the magnitude of the isocurvature perturbations is high and may induce CMB anisotropies not compatible with the data [131].

The second instance is when smaller structures of antimatter $< 10 - 20$ Mpc are possible. The CMB constraint weakens when decreasing the scale. However, CR and gamma-ray data restricts the number of such smaller antimatter objects, not excluding, however, the possibility for their existence. These structures are constrained mainly from CR and gamma-ray data, and should be studied more precisely. Spatial variations of the light elements are expected also.

For the stochastic+explicit CP-violation case we also explore two possibilities. The first one is if there exist vast matter superclusters with typical scale D at a $L \sim 120$ Mpc separation (as observed), while the antimatter objects are of characteristic scales $d \leq 10^{-4}D$. Hence, depending on the following evolution these antimatter regions may collapse to form small antigalaxies, antistar clusters or vast dense antihydrogen clouds. They are at a safe distance from the matter superclusters at about $l_b \sim 60$ Mpc. All the observational constraints may be satisfied.

The second case is for scales of the antimatter domains are of galaxy cluster or galaxy scales. Different possibilities for antimatter domains may be realized, namely between galaxy clusters an antimatter galaxy may wonder, in the space between groups of galaxies a globular star anticluster may be found.

It will be subject of our future works to explore this theme more precisely.

In conclusion, we followed numerically the evolution of the scalar field and baryon charge for the period after inflation until the B-conservation epoch and calculated their final values for different values of the gauge coupling constant α , Hubble constant during inflation H_I , mass of the condensate m and self coupling constants λ_i . We analysed and discussed the evolution of $\varphi(t)$ and $B(t)$ and the final B value dependence on the parameters of the model. We showed that in the frame of our model it is possible to produce the observed matter-antimatter asymmetry.

6.4 Discussion and conclusions

We have investigated the experimental and observational evidences for an existence of antimatter in the vicinity of our Galaxy. We have studied the available data from Cosmic and Gamma rays and have compared them with the theoretical predictions. Our analysis confirms that there is no significant amounts of antimatter up to the distance of 10 - 20 Mpc from CR. Therefore, it is possible to have large antimatter structures safely separated from the matter ones at large distances and it is interesting to study a baryogenesis model, which can predict this.

We have provided precise numerical analysis of the SFC baryogenesis model numerically accounting for the particle creation processes. We have compared it with the analytical calculation and showed that it is important to use a numerical approach to calculate Γ instead of the analytical estimations because of the considerable difference in the obtained results.

We have investigated the dependence of the field and baryon charge evolution and their final values on the model's parameters α , H , m , λ_i . Qualitative dependences of the final B on the model parameters have been found:

The results can be used to determine the range of the values of the model's parameters, necessary to produce the baryon asymmetry β , consistent with the observed one. Our preliminary analysis shows that for a natural range of SCB model's parameters, a value of β higher by an order of magnitude or two (depending on the parameters) than the observed one is obtained. This result points to the necessity of processes, diluting the produced β at BC epoch to its observed today value.

The results of this analysis may be used for constructing successful baryogenesis models in future studies. Moreover, assuming that SCM is the nature chosen baryoge-

nesis, from the observed value of the baryon asymmetry it is possible to put cosmological constraints on the SUSY parameters within a concrete inflationary scenario, or/ and fixing the SUSY mass and couplings, it is possible to point to the preferable inflationary model.

Our preliminary analysis of the evolution of the spacial distribution of the field shows that the initial natural monotonic distribution of the field due to the unharmonicity of its potential transfers into quasiperiodic distribution. Thus, an initially baryon excess region results into regions with baryon excess and such of baryon underdensities. This result is in accordance with previous surveys of SCB models.

For a natural range of the model's parameters this model is able to predict astronomically interesting vast antimatter domains, separated from the matter ones by baryonically empty voids.

6.5 Future work

Future experiments on long balloon flights and spacecrafts (AMS-02 for instance) may reveal the secrets of nearby (up to 150 Mpc) antiworlds, may choose among the *anti* baryogenesis models and may help fix the parameters of the discussed baryogenesis model.

As a first step of future more precise study, we intend to investigate an inhomogeneous SFC baryogenesis model and possible symmetric matter-antimatter Universe. We will discuss the observational bounds for different cases with matter and antimatter domains, separated on safe distances.

In future it is interesting to develop and numerically explore the SFC inhomogeneous models. It is interesting to study the possibility to produce large antimatter domains, safely separated from the matter ones at large distances in the frame of the discussed above SFC baryogenesis scenario. We plan to calculate numerically the spacial distribution of the baryon charge for the baryon conservation time obtaining it from $B(t)$ evolution for different initial values of the field, corresponding to its initial spacial distribution $\varphi(t_i, r)$. The observed spacial distribution of the visible matter at present is defined by the spacial distribution of the baryon charge of φ at the moment of baryogenesis t_B , $B(t_B, r)$. It will be useful to obtain estimations for scales of mat-

6.5 Future work

ter and antimatter domains and the distances between them for different sets of the parameters of our model.

Main results and contributions

In this thesis we have discussed physical processes effecting the generation of the baryonic matter content of the Universe. First, we have studied the processes important for the chemical content of the baryonic component of the Universe, namely Big Bang Nucleosynthesis during which several light elements have been formed. We have studied the role of $\nu_e \leftrightarrow \nu_s$ neutrino oscillations on the ${}^4\text{He}$ production and have obtained cosmological bounds on the neutrino oscillations parameters. The obtained results are important for revealing neutrino properties, and are useful for defining the cosmological role of the sterile neutrino, as well as for constraining different models predicting the presence of sterile neutrinos in the early Universe.

Further we have studied the processes effecting the generation of the baryon content of the Universe, namely Baryogenesis and have examined a baryogenesis model, based on the Affleck-Dine scenario. We have provided a numerical analysis, accounting for the particle creation processes from the damping scalar field and have studied the dependence of the evolution of the field and baryon charge, contained in it on the model parameters.

The main contributions, presented in the PhD thesis are:

1. We have provided detail numerical analysis of the BBN production of ${}^4\text{He}$, Y_p , in the presence of $\nu_e \leftrightarrow \nu_s$ neutrino oscillations, effective after electron neutrino decoupling, accounting for all known oscillations effects on cosmological nucleosynthesis at the following model parameters: $\delta m^2 = [10^{-7} - 10^{-9}]$ and for all θ .
2. We have studied the role of non empty ν_s state, $\delta N_s \neq 0$, obtaining numerically ${}^4\text{He}$ production in the frames of the model of BBN with $\nu_e \leftrightarrow \nu_s$ neutrino oscillations for $\delta N_s = 0; 0.5; 0.7; 0.9$.

3. We have calculated iso-helium contours for $\delta Y_p/Y_p = 5.2\%$ for $\delta N_s = 0; 0.5; 0.7; 0.9$, both for resonant and non-resonant oscillations.
4. Following the current available observational data for ${}^4\text{He}$ abundance, we have obtained cosmological bounds on oscillation parameters with initially empty sterile state $\delta N_s = 0$ and with initially partially filled sterile state $\delta N_s = 0.5; 0.7; 0.9$, corresponding to $\delta Y_p/Y_p = 5.2\%$. Analytical fits to the exact constraints for $\delta N_s = 0$ and $\delta Y_p/Y_p = 5.2\%$ have been calculated.
5. We have studied the cosmological constraints dependence on the neutrino oscillations parameters, corresponding to $\delta Y_p/Y_p \geq 5\%$ and δN_s : it has been found that the cosmological constraints on oscillation parameters relax with the increase of δN_s till $\delta N_s = 1$, when they are alleviated.
6. We have constructed Scalar field condensate (SFC) baryogenesis model based on Affleck and Dine baryogenesis scenario, which is consistent with the low energy scales required by inflation.
7. We have developed a numerical procedure for accounting of the particle creation processes of damping scalar field $\varphi(t)$ and for studying the dependence of the evolution of $\varphi(t)$ and $B(t)$ on the model parameters.
8. We have examined the role of the particle creation processes on the evolution of $\varphi(t)$ and $B(t)$. We have shown that there is a considerable difference in the obtained results compared to the analytical approach for Γ calculation - 2 orders of magnitude. Therefore, a numerical account is necessary to investigate more precisely the processes of the field and baryon charge evolution in the frames of the model.
9. We have numerically obtained the dependence of the field and baryon charge evolution and their final values on the model's parameters α , H , m , λ_i . The results could be used for construction of baryogenesis models based on the Affleck and Dine scenario.
10. We have studied the available data from Cosmic rays for \bar{p} , \bar{D} , ${}^4\bar{He}$ from BESS, CAPRICE, MASS, PAMELA, AMS-01, AMS-02 experiments in order to examine the possibility of existence of the significant antimatter regions in the Universe.

List of publications

Publications in journals

- Kirilova D., **Panayotova M.**, The Role of Particle Creation Processes in the Scalar Condensate Baryogenesis Model, *Bulg. J. Phys.*, 34 no.s2 (2007), 330-335
- Kirilova D., **Panayotova M.**, Relaxed big bang nucleosynthesis constraints on neutrino oscillation parameters, *JCAP12* (2006) 014
- **Panayotova M.**, General BBN bounds on electron-sterile neutrino oscillations, *Bulg. J. Phys.* 38 (2011) 341-345
- **Panayotova M.**, Kirilova D., The dependence of the baryon asymmetry generation on the couplings of the baryon charge carrying scalar field, *Bulg. J. Phys.* 20 (2014) 45-50

Abdus Salam ICTP publications

- Kirilova D., **Panayotova M.**, More General BBN Constraints on Neutrino Oscillations, 2004 ICTP report IC/IR/2004/13, p. 1-6
- D. Kirilova, **M. Panayotova**, The Role of Particle Creation Processes in the Scalar Condensate Baryogenesis Model, ICTP Internal Report, IC/IR/2006/009, Trieste, Italy.

Conference proceedings

- Kirilova D., **Panayotova M.**, Valchanov T., Vast antimatter regions and SUSY-condensate baryogenesis, 2002, Chatteau de Blois, France, ed. L. Inconomidou-Fayard and J. Tran Thanh Van, THE GIOI publishers, astro-ph/0209605 (extended version). Proc. XIVth Rencontres de Blois "Matter-Antimatter Asymmetry" 16th-22nd June, 2003, p. 439-442

- Kirilova D., **Panayotova M.**, Cosmological constraints on neutrino oscillations for initially non-zero sterile state, 2004, Proc. 4th Serbian-Bulgarian Astronomical Conference (IV SBGAC), Belgrade, Serbia 21-24 April, eds. M. Dimitrievich, V. Golev, L. Popovic and M. Tsvetkov, Publ. Astron. Soc. Rudjer Boskovic 5, 2005, p. 201-207
- Kirilova D., **Panayotova M.**, Inhomogeneous baryogenesis model and antimatter in the Universe, Proc. 8th Serbian-Bulgarian Astronomical Conference (VIII SBGAC), Leskovac, Serbia 8-12 May, v.12, 249-256, 2013

Abstracts

- Kirilova D., **Panayotova M.**, Cosmological Constraints on Neutrino Oscillations for Initially Non-Zero Sterile State, Non-acelerator astroparticle physics, eds. A. Carrigan, G. Giacomelli, N. Paver, World Scientific, 2005, p. 301
- Kirilova D., **Panayotova M.**, Inhomogeneous Baryogenesis model and antimatter in the Universe, Book of Abstracts, VIII Serbian-Bulgarian Astronomical Conference, Belgrade, 2012, eds. M. Dmitrijevic, M. Tsvetkov, p. 47-48

Citations

Kirilova D., Panayotova M., Relaxed big bang nucleosynthesis constraints on neutrino oscillation parameters, JCAP12 (2006) 014

Citations:

1. Lesgourgues J., Pastor S., Neutrino mass from Cosmology, Adv. High Energy Phys. (2012) 608515
2. Mangano G., et. al., Updated BBN bounds on the cosmological lepton asymmetry for non-zero θ_{13} , Phys.Lett. B708 (2012) 1-5
3. Iocco F., et. al., Primordial Nucleosynthesis: from precision cosmology to fundamental physics, Phys. Rept. 472 (2009) 1-76
4. Harries N. P., The Effect of primordial fluctuations on neutrino oscillations, OOTP-08-03-P, CERN-PH-TH-2008-015 (2008), arXiv:0801.3742
5. Chu Y., Cirelli M., Sterile neutrinos, lepton asymmetries, primordial elements: How much of each?, Phys.Rev. D74 (2006) 085015

Autocitations:

1. Kirilova D., Lepton Asymmetry and Neutrino Oscillations Interplay, Hyperfine Interact. 215 (2013) 1-3, 111-118
2. Kirilova D., Chizhov M., BBN constraints on neutrino and CNB, Prog. Part. Nucl. Phys. 64 (2010) 375-377
3. Kirilova D., From Mateev's baryogenesis ideas to contemporary cosmological constraints, Bulg.J.Phys. 38 (2011) 242-25

4. Kirilova D., BBN with Late Electron-Sterile Neutrino Oscillations: The Finest Leptometer, JCAP 1206 (2012) 007
5. Kirilova D., Non-equilibrium Neutrino In The Early Universe Plasma, Conf. Proc., 1121, School and Workshop on Space Plasma Physics, 31.08- 07.09, Sozopol, Bulgaria, ed. I. Zhelyazkov, 2009, 83-89. ISSN 0094-243X
6. Kirilova D., On Lepton Asymmetry and BBN, Progress in Particle and Nuclear Physics, Physics 66 (2011) 260-265
7. Kirilova D., Frere J. M., Neutrino in the Early Universe, ULB-TH/12-03, New Astronomy Reviews v.56, issue 6 (2012) 169-180
8. Kirilova D., Neutrino in the Universe, Bulg. Astr. J. 10 (2008) 1-9
9. Kirilova D., More General BBN Constraints on Neutrino Oscillations Parameters - Relaxed or Strengthened, IJMPD 16 (2007) 7, 1-14

Kirilova D., Panayotova M., Valchanov T., Vast antimatter regions and SUSY-condensate baryogenesis, 2002, Chatteau de Blois, France, astro-ph/0209605 (extended version). Proc. XIVth Rencontres de Blois "Matter-Antimatter Asymmetry" 16th-22nd June, 2003, 439-442

Citations:

1. Alpat B., Astroparticle Physics with AMS02, arXiv:0707.3605 (2007)
2. Dolgov A. D., Cosmological matter antimatter asymmetry and antimatter in the universe, to appear in the proceedings of Conference: C02-06-16 (2002), hep-ph/0211260

Panayotova M., General BBN bounds on electron-sterile neutrino oscillations, Bulg. J. Phys. 38 (2011) 341-345

Citations:

1. Kirilova D., Lepton Asymmetry and Neutrino Oscillations Interplay, Hyperfine Interact. 215 (2013) 1-3, 111-118
2. Kirilova D., From Mateev's baryogenesis ideas to contemporary cosmological constraints, Bulg. J. Phys. 38 (2011) 242-25

3. Kirilova D., Frere J. M., Neutrino in the Early Universe, ULB-TH/12-03, New Astronomy Reviews v.56, issue 6 (2012) 169-180
4. Kirilova D., BBN with Late Electron-Sterile Neutrino Oscillations: The Finest Leptometer, JCAP 1206 (2012) 007

Kirilova D., Panayotova M., The Role of Particle Creation Processes in the Scalar Condensate Baryogenesis Model, Bulg. J. Phys., 34 s2 (2007), 330-335

Autocitations:

1. Kirilova D., From Mateev's baryogenesis ideas to contemporary cosmological constraints, Bulg. J. Phys. 38 (2011) 242-25
2. Kirilova D., Panayotova M., Inhomogeneous baryogenesis model and antimatter in the Universe, Proc. 8th Serbian-Bulgarian Astronomical Conference (VIII SBGAC), Leskovac, Serbia 8-12 May, Publ. Astron. Soc. Rudjer Boskovic N11 (2012) 259-264

Kirilova D., Panayotova M., More General BBN Constraints on Neutrino Oscillations, 2004 ICTP report IC/IR/2004/13, 1-6

Autocitations:

1. D. Kirilova, More General BBN Constraints on Neutrino Oscillations Parameters - Relaxed or Strengthened, IJMPD 16 (2007) 7, 1-14
2. Kirilova D., Cosmological Constraints on Neutrino Oscillations - Relaxed or Strengthened, Proc. 6th Intern. Symposium on Frontiers of Fundamental and Computational Physics, 26-29 September, Udine, Italy, Frontiers of Fundamental Physics, eds. B. Sidharth, F. Honsell, A. De Angelis, Kluwer Academic Publishers (2006) 55-59, ICTP report IC/2005/113, 1-5

Appendices

References

- [1] KIRILOVA D.; PANAYOTOVA M. *Bulg. J. Phys.* 34 s2, 330, 2007. [v](#), [vi](#), [49](#), [54](#), [55](#), [56](#), [57](#), [59](#), [60](#), [61](#), [63](#)
- [2] KIRILOVA D.; PANAYOTOVA M. *Bulg. A. J.* 20, 45, 2013. [vi](#), [vii](#), [66](#), [67](#)
- [3] BERINGER J.; ET. AL. (PARTICLE DATA GROUP). *Phys. Rev. D*86, 010001, 2012. [1](#), [10](#), [24](#), [47](#)
- [4] PETTINI M.; COOCE R. *arXiv:1205.3785 [astro-ph.CO]*, 2012. [1](#), [47](#)
- [5] BENNETT C. L.; ET. AL. *arXiv:1212.5225v2*, 2012. [1](#), [10](#), [43](#), [47](#)
- [6] SAKHAROV A. *JETP* 5, 32, 1967. [1](#), [48](#)
- [7] KUZMIN V. A.; RUBAKOV V. A.; SHAPOSHNIKOV M. E. *Phys. Rev. Lett.* 84, 3756, 1985. [1](#), [48](#)
- [8] FUKUGITA M.; YANAGIDA T. *Phys. Lett. B*174, 45, 1986. [1](#), [49](#)
- [9] AFFLECK I.; DINE M. *Nucl. Phys., B*249, 361, 1985. [1](#), [49](#)
- [10] DOLGOV A. D. *arXiv:1002.2940*, 2010. [2](#)
- [11] HAMANN J.; ET. AL. *arXiv:1108.4136*, 2011. [2](#)
- [12] ASAKA T.; SHAPOSHNIKOV M.; KUSENKO A. *Phys. Lett. B*638, 401, 2006. [2](#)
- [13] ABAZADJIAN K.; ET. AL. *arXiv: 1204.5379*, 2012. [2](#)
- [14] HOLANDA P. C.; SMIRNOV A. YU. *Phys. Rev. D*83, 113011, 2011. [2](#)
- [15] DOLGOV A. D. *Sov. J. Nucl. Phys.* 33, 700, 1981. [3](#), [25](#)
- [16] ALPHER R. A.; BETHE H.; GAMOW G. *Phys. Rev. Lett.* 73, 803, 1948. [6](#)
- [17] ALPHER R. A.; HERMAN R. C. *Rev. Mod. Phys.* 22, 153, 1950. [6](#)
- [18] POSPELOV M.; PRADLER J. *Ann. Rev. Nucl. Part. Sci.* 60, 539, 2010. [9](#)
- [19] MANGANO G.; ET. AL. *Nucl. Phys. B* 729, 221, 2005. [10](#), [18](#)
- [20] KOMATSU E.; ET. AL. *Astrophys. J. Supp.* 180, 330, 2009. [10](#)
- [21] WAGONER R. V.; FOWLER W. A.; HOYLE F. *Astrophys. J.* 148, 3, 1967. [10](#)
- [22] COC A.; ET. AL. *Ap. J.* 600, 544, 2004. [10](#)
- [23] CYBURT R. H. *Phys. Rev. D* 70, 023505, 2004. [10](#)

REFERENCES

- [24] SERPICO P. D.; ET. AL. *Int. J. Mod. Phys. A*19, 431, 2004. [10](#)
- [25] IOCCO F.; ET. AL. *Phys. Rept.* 472, 1, 2009. [10](#), [11](#), [12](#), [18](#)
- [26] CYBURT R. H.; FIELDS B. D.; OLIVE K. A. *JCAP* 0811, 012, 2008. [11](#), [18](#)
- [27] PETTINI M.; ET. AL. *MNRAS* 391, 1499, 2008. [11](#)
- [28] GEISS J.; GLOECKLER G. *Space Science Rev.* 130, 5, 2007. [11](#)
- [29] BANIA T. M.; ROOD R. T.; BALSER D. S. *Nature* 415, 54, 2002. [13](#)
- [30] SBORDONE L.; ET. AL. *AA* 522, 26, 2010. [14](#)
- [31] STEIGMAN G. *Proceedings of the 11th Symposium on Nuclei in the Cosmos (NIC XI), to be published by Proceedings of Science*, 2010. [14](#)
- [32] IZOTOV Y. I.; THUAN T. X. *Astrophys. J. Lett.* 710, L67, 2010. [15](#), [16](#), [17](#), [18](#), [34](#)
- [33] PANAYOTOVA M. *Bulg. J. Phys.* 38, 341, 2011. [18](#), [34](#), [35](#), [36](#)
- [34] DOLGOV A. D. *Sov. J. Nucl. Phys.* B506, 7, 1981. [18](#), [29](#)
- [35] KIRILOVA D. *JINR E2-88-301*, 1988. [18](#), [26](#), [29](#)
- [36] BARBIERI R.; DOLGOV A. D. *Phys. Lett.* B237, 440, 1990. [18](#)
- [37] BARBIERI R.; DOLGOV A. D. *Nucl. Phys.* B349, 743, 1991. [18](#)
- [38] STEIGMAN G. *JCAP* 04, 029, 2010. [18](#)
- [39] AVER E.; OLIVE K. A.; SKILLMAN E. D. *JCAP* 05, 003, 2010. [18](#)
- [40] IOCCO F.; ET. AL. PARTHENOPE. *website: <http://parthenope.na.infn.it>*, 2008. [18](#)
- [41] AVER E.; OLIVE K. A.; SKILLMAN E. D. [*arXiv:1012.2385v1*], 2010. [18](#), [34](#)
- [42] COWAN C. L.; REINES JR. F.; HARRISON F. B.; KRUSE H. W.; MCGUIRE A. D. *Science* 124, 103, 1956. [19](#)
- [43] DAVIS R. *Phys. Rev. Lett.* 12, 303, 1964. [19](#)
- [44] CLEVELAND B. T.; ET. AL. (HOMESTAKE). *Ap. J.* 496, 505, 1998. [19](#)
- [45] PONTECORVO B. *Zh. Eksp. Teor. Fiz.* 53, 1717 [*Sov. Phys. JETP* 26, 984, 1967]. [20](#), [22](#)
- [46] FUKUDA Y.; ET. AL. *Phys. Rev. Lett.* 77, 1683, 1996. [20](#)
- [47] ABDURASHITOV J. N. *Phys. Rev.* C80, 015807, 2009. [20](#)
- [48] HAMPEL W.; ET. AL. *Phys. Lett.* B447, 127, 1999. [20](#)
- [49] ALTMANN M.; ET. AL. *Phys. Lett.* B616, 174, 2005. [20](#)
- [50] HOSAKA J.; ET. AL. *Phys. Rev.* D73, 112001, 2006. [20](#)
- [51] AHARMIM B.; ET. AL. *Phys. Rev. Lett.* 101, 111301, 2008. [20](#)

REFERENCES

- [52] AHARMIM B.; ET. AL. *Phys. Rev. C*81, 055504, 2010. [20](#)
- [53] CLARK R.; ET. AL. (IMB). *Phys. Rev. Lett.* 79, 345, 1997. [21](#)
- [54] FUKUDA Y.; ET. AL. (SUPER-KAMIOKANDE COLLAB.). *Phys. Rev. Lett.* 81, 1562, 1998. [21](#)
- [55] ALLISON W. W. M.; ET. AL. *Phys. Lett. B*449, 137, 1999. [21](#)
- [56] AMBROSIO M.; ET. AL. *Phys. Lett. B*517, 59, 2001. [21](#)
- [57] AHN M. H.; ET. AL. (K2K COLLAB.). *Phys. Rev. D*74, 072003, 2006. [21](#)
- [58] ADAMSON P.; ET. AL. (MINOS COLLAB.). *Phys. Rev. Lett.* 101, 131802, 2008. [21](#)
- [59] AGUILAR A.; ET. AL. (LSND). *Phys. Rev. D*64, 112007, 2001. [21](#)
- [60] AGUILAR-AREVALO A.; ET. AL. (MINIBOONE). *Phys. Rev. Lett.* 102, 101802, 2009. [21](#)
- [61] AGUILAR-AREVALO A.; ET. AL. (MINIBOONE). *Phys. Rev. Lett.* 105, 181801; *arXiv:1208.0322*, 2010. [21](#)
- [62] LEP COLLAB.; ET. AL. *Phys. Rept.* 427, 257, 2006. [22](#)
- [63] HAMANN J.; ET. AL. *Phys. Rev. Lett.* 105, 181301, 2010. [22](#)
- [64] KOPP J.; MALTONI M.; SCHWETZ T. *Phys. Rev. Lett.* 107, 091801, 2011. [22](#)
- [65] MAKI Z.; NAKAGAWA M.; SAKATA S. *Prog. Theor. Phys.* 28, 870, 1962. [22](#)
- [66] FOGLI G. L.; ET. AL. *Phys. Rev. D*84, 053007, 2011. [23](#)
- [67] AN F. P.; ET. AL. (DAYA BAY COLL.). *Chin. Phys. C*37, 011001, 2013. [23](#)
- [68] KIRILOVA D.; CHIZHOV M. *Phys. Lett. B*393, 375, 1997. [25](#), [26](#), [28](#), [29](#)
- [69] BILENKI S. M. *JINR P2-83-441*, 1983. [25](#)
- [70] MANOHAR A. *Phys. Lett. B*196, 370, 1987. [25](#)
- [71] DOLGOV A. D. *Phys. Rep.* 370, 333, 2002. [29](#)
- [72] KIRILOVA D.; CHIZHOV M. *Neutrino 96, Helsinki*, 478, 1996. [29](#)
- [73] KIRILOVA D. *Astropart. Phys.* 19, 409, 2003. [29](#), [40](#)
- [74] KIRILOVA D. *Int. J. Mod. Phys. D*13, 831, 2004. [29](#), [30](#), [35](#)
- [75] FOOT R.; THOMSON M.; VLKAS R. *Phys. Rev. D*53, R5349, 1996. [29](#)
- [76] KIRILOVA D. *Cen. Europ. J. of Phys.* 2:3, 467, 2004. [30](#)
- [77] KIRILOVA D.; PANAYOTOVA M. *JCAP* 12, 014, 2006. [31](#), [34](#), [36](#)
- [78] KIRILOVA D.; CHIZHOV M. *Phys. Rev. D*58, 073004, 1998. [30](#), [33](#)
- [79] KIRILOVA D.; CHIZHOV M. *Nucl. Phys. B*591, 457, 2000. [30](#), [33](#)
- [80] KIRILOVA D.; CHIZHOV M. *Nucl. Phys. Suppl. B*100, 360, 2001. [30](#), [33](#)
- [81] KIRILOVA D. *Int. J. Mod. Phys. D*163, 1, 2007. [31](#), [34](#), [37](#)

REFERENCES

- [82] KIRILOVA D. *Int. J. Mod. Phys. D13*, 831, 2003. [34](#)
- [83] KIRILOVA D.; PANAYOTOVA M. *Proc. 4th Serbian-Bulgarian Astronomical Conference (IV SBGAC), Belgrade, Serbia 21-24 April, 201*, 2004. [34](#), [35](#), [38](#)
- [84] KIRILOVA D.; PANAYOTOVA M. *IC/IR/2004/13*, 1, 2004. [34](#)
- [85] KIRILOVA D.; PANAYOTOVA M. *Proc. VIIIth school Non-accelerator astroparticle physics, Trieste, 301*, 2004. [34](#)
- [86] KIRILOVA D. *ULB-TH/04-01*, ULB, 2004. [34](#)
- [87] AGE P. A. R.; ET. AL. (PLANCK COLLAB.). *arXiv:1303.5077 [astro-ph.CO]*, 2013. [43](#), [47](#)
- [88] ABE K.; ET. AL. *Phys. Lett. B670*, 103, 2008. [44](#)
- [89] ORMES J.; ET. AL. *Ap. J.* 482, L187, 1997. [44](#)
- [90] MATSUNAGA H.; ET. AL. *Phys. Rev. Lett.* 81, 4052, 1998. [44](#)
- [91] ORITO S.; ET. AL. *Phys. Rev. Lett.* 84, 1078, 2000. [44](#)
- [92] MAENO T.; ET. AL. *Ap. Phys.* 16, 121, 2001. [44](#)
- [93] ASAOKA Y.; ET. AL. *Phys. Rev. Lett.* 88, 051101, 2002. [44](#)
- [94] WIZART/CAPRICE COLLAB. *ApJ* 561, 787, 2001. [44](#)
- [95] HOFF M.; ET. AL. *ApJ* 467, L33, 1996. [44](#)
- [96] BIEBER J. *Phys. Rev. Lett.* 83, 674, 1999. [44](#)
- [97] ULLIO P. BERGSTROM L., EDSJO J. *ApJ* 526, 215, 1999. [44](#)
- [98] DONATO F.; ET. AL. *ApJ* 563, 172, 2001. [44](#)
- [99] KIRILOVA D.; PANAYOTOVA M.; VALCHANOV T. *Proc. XIVth Rencontres de Blois "Matter-Antimatter Asymmetry" 16th-22nd June, 2003, p.439; IC/2002/133*, 2002. [45](#), [46](#), [49](#), [50](#), [65](#)
- [100] CHARDONNET P.; ORLOFF J.; SALATI P. *Phys. Lett. B* 409, 313, 1997. [44](#)
- [101] AGUILAR A.; ET. AL. (LSND). *Phys. Rep.* 366 (6), 331, 2002. [44](#)
- [102] MAYOROV A. G.; ET. AL. *JETP Lett.* 93 (11), 628, 2011. [44](#)
- [103] CASADEI D. *arXiv:astro-ph/0404529v1*, 2004. [44](#)
- [104] AGUILAR M.; ET. AL. (AMS). *Phys. Rev. Lett.* 110, 141102, 2013. [46](#)
- [105] STECKER F.; ET. AL. *Phys. Rev. Lett.* 27, 1469; *hep-ph/0207323*, 1971; 2002. [46](#)
- [106] STEIGMAN G. *Ann. Rev. Astr. Astrop.* 14, 339,, 1976. [46](#)
- [107] DUDAREVICH A.; WOLFENDALE A. *MNRAS* 268, 609, 1994. [46](#)
- [108] COHEN A.; ET. AL. *Ap. J.* 495, 539, 1998. [46](#), [68](#)
- [109] DOLGOV A. D.; KIRILOVA D. *J. Moscow Phys. Soc.* 1, 217, 1991. [46](#), [49](#), [50](#), [54](#), [55](#)

REFERENCES

- [110] REIMER O.; ET. AL. *Astrophys. J.* 588, 155, 2003. 46
- [111] FERMI LAT. *Phys. Rev. Lett.* 104, 101101, 2010. 46
- [112] SAKHAROV A.; KHOLOPOV M.; RUBIN S. *International Errophysics Conference on HEP, hep2002/212; astro-ph/0111524*, 1967. 46
- [113] BELOTSKY K.; ET. AL. *Yad. Phys.* 63, 290, 2000. 46
- [114] CHECHETKIN V.; ET. AL. *Phys. Lett. B* 118, 329, 1982. 47
- [115] KURKI-SUNIO H.; SIHVOLA E. *Phys. Rev. Lett.* 84, 3756, 2000. 47
- [116] DOLGOV A. D.; ZELJDOVICH YA.; SAZHIN M. *Cosmology of the Early Universe, Moscow*, 1988. 48
- [117] DOLGOV A. D.; ZELJDOVICH YA. *Rev. Mod. Phys.* 53, 1, 1981. 48
- [118] KLINKHAMER F. R.; MANTON N. S. *Phys. Rev. D* 30, 2212, 1984. 48
- [119] DOLGOV A. D.; KIRILOVA D. *Yad. Phys.* 51 273, 335; *Sov. J. Nucl. Phys.* 51, 172, 1990. 49, 54
- [120] CHIZHOV M.; KIRILOVA D. *AATr*, 10, 69, 1996. 49, 50, 54, 68
- [121] KIRILOVA D.; CHIZHOV M. *MNRAS*, 314, 256, 2000. 49, 69
- [122] KIRILOVA D.; PANAYOTOVA M. *ICTP report IC/IR/2006/009* , 1, 2006. 49, 55, 59
- [123] KIRILOVA D.; PANAYOTOVA M. *Proc. 8th Serbian-Bulgarian Astronomical Conference (VIII SBGAC), Leskovac, Serbia 8-12 May, 2012*, 2012. 49, 55, 58, 59, 62, 64, 65
- [124] VILENKIN A.; FORD L. *Phys. Rev. D* 26, 1231, 1982. 49
- [125] LINDE A. D. *Phys. Lett. B* 116, 335, 1982. 49
- [126] BUNCH T. S.; DAVIES P. C. W. *Proceedings of the Royal Society of London. A. Mathematical and Physical Sciences* 360, 117, 1978. 49
- [127] STAROBINSKY A. A. *Phys. Lett. B* 117 (3-4), 175, 1982. 49
- [128] CHIZHOV M.; DOLGOV A. *Nucl. Phys. B* 372, 521, 1992. 50, 65
- [129] DOLGOV A. D. *Phys. Rep.* 222, 309, 1992. 50
- [130] PRESS W.; ET. AL. *Numerical Recipes in Fortran 77, Second edition, Cambrige Univ. Press*, 2001. 53
- [131] ENQVIST K.; KURKI-SUONIO H.; VALIVIITA J. *PRD* 26, 103003, 2000. 69

=